J Comp Physiol A (1999) 184: 609–630

ORIGINAL PAPER

P. K. Stoddard · B. Rasnow · C. Assad

Electric organ discharges of the gymnotiform fishes: III. *Brachyhypopomus*

Accepted: 22 September 1998

Abstract We measured and mapped the electric fields produced by three species of neotropical electric fish of the genus *Brachyhypopomus* (Gymnotiformes, Rham phichthyoidea, Hypopomidae), formerly *Hypopomus*. These species produce biphasic pulsed discharges from myogenic electric organs. Spatio-temporal false-color maps of the electric organ discharges measured on the skin show that the electric field is not a simple dipole in *Brachyhypopomus*. Instead, the dipole center moves rostro-caudally during the 1st phase (P1) of the electric organ discharge, and is stationary during the 2nd phase (P2). Except at the head and tip of tail, electric field lines rotate in the lateral and dorso-ventral planes. Rostro-caudal differences in field amplitude, field lines, and spatial stability suggest that different parts of the electric organ have undergone selection for different functions; the rostral portions seem specialized for electrosensory processing, whereas the caudal portions show adaptations for d.c. signal balancing and mate attraction as well. Computer animations of the electric field images described in this paper are available on web sites *http://www.bbb.caltech.edu/ElectricFish* or *http://www.fiu.edu/~stoddard/electricfish.html*.

P.K. Stoddard (✉)
Department of Biological Sciences,
Florida International University,
Miami, FL 33199, USA
e-mail: stoddard@fiu.edu
Fax: +1-305-348-1869

B. Rasnow · C. Assad
Divisions of Biology and Electrical Engineering,
California Institute of Technology,
Pasadena, CA 91125, USA

B. Rasnow
Amgen, One Amgen Center Drive,
Thousand Oaks, CA 91320, USA

C. Assad
Jet Propulsion Laboratory,
MS 303-300, 4800 Oak Grove Drive,
Pasadena, CA 91109, USA

Key words Bioelectricity · Communication · Electric fish · Electrogenesis · Electroreception

Abbreviations *EOD* electric organ discharge · *IPI* interpulse interval · *LEA* length to end of anal fin · *P1* phase 1 of EOD · *P2* phase 2 of EOD · *rms* root mean square

Introduction

Over the past four decades, scientists have discovered an unexpected diversity and abundance of electrogenic fishes in the fresh waters of the New World tropics and West Africa. Of particular interest to comparative neurobiologists is the diversity of electric organ discharge (EOD) waveforms produced by these fish for active electrolocation and communication. Because electrolocation appears to have been the driving force behind the evolution of electric signals in the gymnotiforms, we assume that the demands of electrolocation in different ecological niches are probably responsible for much of the EOD variation seen in modern gymnotiform taxa. We do not rule out, a priori, the possibility that gross EOD variation has resulted from genetic drift as much as from functional adaptation. We would argue that regardless of its evolutionary origins, the structure of the EOD constitutes each individual's immediate sensory world, and must be reflected in its strategies for electrolocation, communication, and electrosensory processing.

Active electrolocation and courtship behavior in gymnotiform fishes occur within some fraction of a body length from the fish (Bastian 1976b; Hagedorn and Heiligenberg 1985; Stoddard et al. 1996). In most species, the near electric fields have been found to be far more heterogeneous than would be expected from the simple dipolar EOD waveforms measured beyond a body length (Bennett 1961; Bastian 1976a; Caputi et al. 1989; Rasnow et al. 1993; Rasnow and Bower 1996). To understand electrolocation and close-range communi-

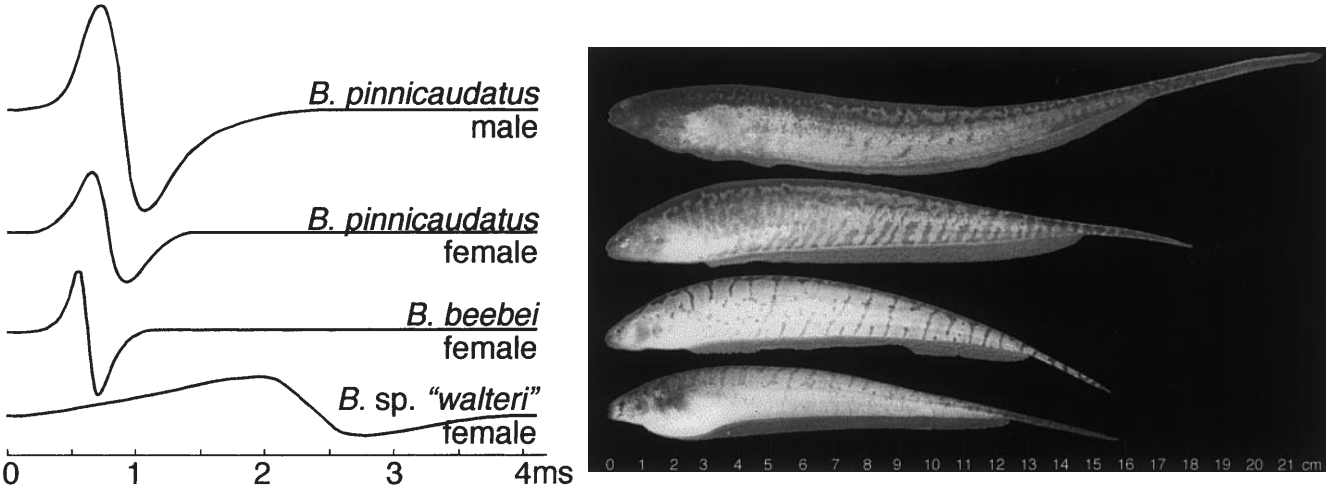

Fig. 1 Remote electric organ discharges (EODs) of the three *Brachyhypopomus* species presented in this study. The photo scale is in centimeters. EODs, shown to the same amplitude scale, were digitized during the daytime from unsedated fish centered lengthwise in an aquarium $120 \times 44 \times 44$ cm. Differential recording electrodes were located on opposite walls 120 cm apart. The photographs are of different individuals than those that we mapped, although they are similar in size and remote EOD waveform. The *B.* sp. *"walteri"* female shown here is noticeably gravid, whereas those we mapped became gravid only subsequent to mapping

cation, we must distinguish between local and remote electric currents and field vectors, much as scientists have distinguished between near-field and far-field acoustic effects in the exploration of auditory processes. Understanding variation in local currents is a key step towards understanding the mechanisms involved in electric imaging of nearby objects as well as the secondary electrosensory strategies of communication and concealment from predators.

This paper is the third in our series on the fine spatiotemporal structure of EODs of the gymnotiform fishes. Our previous studies examined electric field structure generated by the gymnotiform fishes in the families Apteronotidae (Rasnow et al. 1993; Rasnow and Bower 1996) and Eigenmanniidae (Assad et al. 1998). This paper is the first to map systematically the electric fields generated by fish of a gymnotiform family with a pulse-type EOD. Members of the family Hypopomidae produce EODs with a wide range of macrovariation, ranging from one to five distinct peaks or phases. Most Hypopomid species produce a biphasic EOD (Fig. 1). *Brachyhypopomus*, the largest genus in this family, has received much attention for the sexual variation in its usually biphasic waveform (Hagedorn 1986, 1988, 1995; Hagedorn and Zelick 1989; Shumway and Zelick 1988; Westby 1988; Kawasaki and Heiligenberg 1989; Comfort 1990; Hopkins et al. 1990; Hopkins 1991; Franchina and Stoddard 1999). The electric potential of the biphasic EOD of *Brachyhypopomus* first becomes positive at the head and negative at the tail. This portion of the EOD is referred to as the "1st phase" or P1. The second portion, in which the polarities reverse, is referred to as the "2nd phase" or P2. In most species of *Brachyhypopomus*, the 2nd phase of the male's EOD is longer than the female's. Male *Brachyhypopomus* modulate the magnitude and duration of their EODs between day and night and in response to changing social conditions (Hagedorn and Zelick 1989; Hagedorn 1995; Franchina et al. 1998; Franchina and Stoddard 1999). Changes in the EOD appear to stem from changes in local action potentials under the regulation of hormones (Hagedorn and Carr 1985). Thus, *Brachyhypopomus* shows significant promise as a model for exploration of behavioral and hormonal control of action potential waveforms. Based on the assumption that *Brachyhypopomus* is capable of discriminating species and sex differences in its pulsed EOD waveform, the genus *Brachyhypopomus* has also received attention as a model system for discrimination of transient waveforms (Heiligenberg and Altes 1978, Hopkins and Westby 1986, Shumway and Zelick 1988).

The genus *Brachyhypopomus* includes all species formerly in genus *Hypopomus* except a couple of species from the coastal streams of the Guianas typified by *H. artedi* (Mago-Leccia 1994). Members of the genus *Brachyhypopomus* inhabit slow-moving or still waters of the neotropics from Costa Rica to Argentina (Sullivan 1997). Electric discharge rates during normal nocturnal activity range from 8 to 70 EODs s^{-1} for different members of the genus, dropping to less than half that during the day when they are inactive. EOD duration ranges from about 0.5 ms to 5 ms across species, correlating roughly with the interpulse interval (IPI) (Hopkins and Heiligenberg 1978). Congeners with widely varying EOD characteristics frequently inhabit the same bodies of water (Hopkins and Heiligenberg 1978; Hagedorn and Keller 1996; Crampton 1998).

The electric organ of *Brachyhypopomus* is a bilateral structure of myogenic origin. The electrocytes constituting the electric organ are box-shaped cells, innervated only on their posterior surface by cholinergic spinal motor afferents (Fig. 2; Bennett 1961, 1971). Electro-

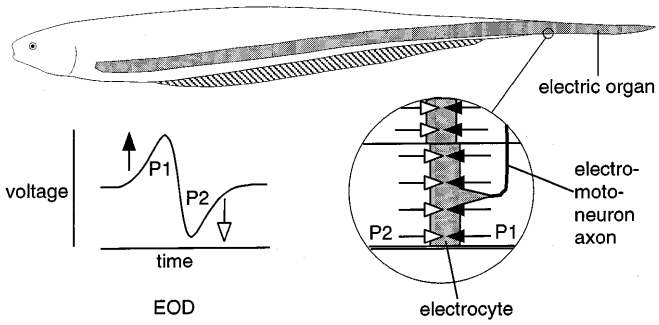

Fig. 2 Schematic of *B. pinnicaudatus* showing the location and extent of the electric organ. A single electrocyte from the posterior region of the electric organ is shown below, innervated by spinal electromotoneurons on its posterior face. Electromotoneurons trigger an action potential in the posterior face of the electrocyte, producing a headward sodium current indicated here by *arrows with filled heads*. These action potentials sum across all the electrocytes in the electric organ to produce the head-positive phase of the EOD (*P1*). Depolarization of the electrocyte interior by P1 triggers a subsequent action potential in the anterior face of the electrocyte, producing a tailward sodium current, indicated here by *arrows with filled heads*. These action potentials sum to produce the head-negative phase of the EOD (*P2*). All electrocytes fire action potentials on their innervated posterior faces but only the more caudal electrocytes fire action potentials on their anterior non-innervated surface as well (Bennett 1961, 1971)

cytes are organized in three to five lengthwise columns, extending from the fish's opercular region, along the ventrolateral sides, to the tip of the caudal filament (Fig. 2; Bennett 1961, 1971; Hopkins et al. 1990; Comfort 1990). EODs measured remotely (hereafter "remote EODs") are biphasic in all but one or two members of the genus (Fig. 1). Electromotoneurons trigger action potentials at the posterior electrocyte surfaces (Bennett 1961, 1971). Summation of these action potentials produces a head-positive, tail-negative electric field in the water around the fish. As the initial head-positive potential subsides, the non-innervated, anterior membranes discharge, producing a head-negative, tail-positive electric field around the fish.

The local structure of the EOD was already known to be complex, varying in waveform, spectrum, and amplitude from head to tail. Bennett (1961) and Bastian (1976a) measured the EOD potential at 10- to 15-mm intervals along the midline of non-curarized *Brachyhypopomus* species with monophasic and biphasic EODs. Their published figures show a significant contrast in spatial complexity between the monophasic and biphasic species. In the monophasic species, the electric potential waveforms measured near the skin were fairly uniform in shape and similar to the EOD measured remotely. In the biphasic species, waveforms measured along the body's surface were very different in shape from the remote EOD and from each other as well. Bennett (1961, 1971) proposed that spatial heterogeneity resulted from differences in electrocyte excitability; more rostral electrocytes discharge only their innervated posterior faces, whereas more caudal electrocytes discharge the non-innervated anterior face as well. Bastian (1976a) inferred that spectral differences in the local EOD resulted from temporal asynchrony of several spatially heterogeneous local currents.

These findings of local EOD heterogeneity have significant implications for electroreception in the contexts of active electrolocation, communication, and passive detection of conspecifics. Variation in local EOD currents will affect the electric images of local objects. For communication and passive detection of other electric fishes, the perceived EOD of a remote fish will be very different in structure from that of a fish close by.

Further use of the genus *Brachyhypopomus* as a model system for waveform control and transient analysis depends on a better understanding of its electric field structure. We present in this paper detailed representations of the electric fields of individuals of three species of *Brachyhypopomus*. Using a robotic electric field measurement system (Rasnow et al. 1993) we obtained detailed electric field maps from fish rendered motionless with the tranquilizer etomidate, a drug that does not interact with the electric organ.

Materials and methods

Most of the materials and methods in these mapping experiments are similar to those described previously (Rasnow et al. 1993; Rasnow 1994; Rasnow and Bower 1996; Assad et al. 1998). We give a brief overview of methods previously described and describe the differences in detail.

Subjects

We mapped EODs from three of four members in a well-resolved clade of *Brachyhypopomus* (Sullivan 1997). Two of these, *B. beebei* (Schultz) and *B. pinnicaudatus* (Hopkins) are sister taxa. The third species, *B.* sp. nov. *walteri*, is described by Sullivan (1997), but the description is not yet published. We obtained juvenile *B. beebei* and *B.* sp. "*walteri*" from the Amazon basin via a Peruvian importer in Miami, and raised them to adulthood in the laboratory at a water conductivity of 100 μS cm^{-1}. We mapped the electric fields of mature females of these two species, one 145-mm *B. beebei*, and two 144-mm *B.* sp. "*walteri*".

A breeding colony of "feather-tailed knifefish" (*B. pinnicaudatus*) was established at FIU from eggs of Argentinean parent stock. We chose a mature, non-gravid female for measuring effects of temperature on the EOD, and mature fish of both sexes for exploring sex differences in the EOD. Female *Brachyhypopomus* are better subjects for electric field mapping than males because their EODs are more stable (Franchina and Stoddard 1999). Electric field mapping measurements take about 4 h to complete, whereas the EOD duration and amplitude of a male *B. pinnicaudatus* can change by 25–35% in 2 h (Franchina and Stoddard 1999).

Effects of temperature on the EOD

We determined the effect of temperature on the EOD by placing mature *B. pinnicaudatus* females in an aquarium at 20 °C and raising the temperature to 30 °C over the course of 2 h. The fish was restricted to a mesh sleeve in the center of a 115-l aquarium (95 × 35 × 40 cm). Water conductivity was 119 μS cm^{-1} (8.4 kΩ-cm). EODs detected with silver ball electrodes situated at either end of the tank were amplified differentially (CWE bioamplifier BMA-

200, a.c.-coupled, 10 kHz Butterworth 2-pole low-pass filter) and digitized at 48,000 samples s^{-1}, 16 bits (Digidesign Audiomedia II A/D converter in an Apple Power Macintosh). We calculated EOD durations from interpolated thresholds 5% above and below the baseline. All analyses described in this paper were conducted using MATLAB (The Mathworks).

Mapping the electric field

Mapping 1: water conditions

We held water temperature constant during the mapping procedure by keeping the room temperature at 28 °C. We standardized water conductivity at 200 μS cm^{-1} and held the fish at this conductivity for 2 weeks prior to mapping. This conductivity is higher than that typical of the streams where these fish live (Crampton 1996) but we selected a higher conductivity to constrain the spread of the electric field so that we might minimize distortion caused by the tank walls. Therefore, our measurements of absolute field strength at a given distance from the fish may be different than would be measured in the field.

Mapping 2: positioning the fish

During the mapping procedure, we supported the fish in the center of the 60 × 60 × 18 cm measurement tank on thin, plastic-coated wires that allowed their bodies to be oriented normally for mapping of the lateral plane and body surface, or on their sides while mapping the dorsal and ventral planes. The fish were tranquilized by a steady infusion of (+)etomidate, a GABA binding enhancer (Ticku 1983), delivered at 1–3 ppm in the respirator water. Etomidate at these concentrations had no discernible effect on the structure of the EOD as measured remotely. The rate of discharge dropped by about 50%, consistent with the known GABAergic inhibition of the *Brachyhypopomus* pacemaker neurons by the PPn-I region of the prepacemaker nucleus (Kawasaki and Heiligenberg 1990; Kennedy and Heiligenberg 1994).

Mapping 3: measurement apparatus

A computer-controlled XY plotter arm moved an electrode array around a plane of the measurement tank. To measure electric fields we used an array of four glass-coated electrodes, with 150- to 250-μm-diameter silver tips arranged approximately along the three orthogonal axes of a 1-mm cube. Calibration of the array geometry to a precision of 10s of microns is described by Rasnow and Bower (1996). A stationary electrode sampled the EOD at the same time as the moving electrode array and thus served as a reference for subsequent phase alignment of EODs measured in different locations in the tank. EODs were amplified and digitized simultaneously with 16-bit resolution on all five channels at 48,000 samples s^{-1} per channel (see Rasnow et al. 1993).

Mapping 4: temporal alignment of digitized EODs

We time-aligned the sampled EODs by aligning precisely each of the EODs digitized on the stationary reference electrodes using the following process: (1) up-sampling the reference channel data five times, (2) cross-correlating each reference channel with a master reference, (3) least-squares fitting the cross correlation at points nearest the peaks to a parabola, and solving for the maxima whose location corresponds to optimal latency (4), then frame-shifting all five channels of synchronously sampled data by that latency, using a cubic spline to interpolate time-shifted voltages between measured data points. This alignment method is robust to measurement noise and requires no additional filtering of the data because the cross-correlation does an amplitude-weighted average over the entire EOD. Alignment in this manner generally achieved submicrosecond phase resolution.

Mapping 5: stability and noise of the reference channel

We can assess the constancy of the EOD and our success in alignment by considering the stability of the EOD digitized on the stationary reference channel. The standard deviation of the reference channel (Fig. 3A, B) was larger during the 1st phase than the 2nd phase. Standard deviation of the amplitude of this phase was 0.005 times the peak amplitude; coefficients of variation of the main peaks are about 0.0025. Noise on the reference channel measured 0.9–1.0 μV rms, of which 0.4 μV is attributable to Johnson noise of the electrodes and much of the rest to 60 Hz and harmonics from the power lines. We had too few sample points to remove the line noise analytically. These values are what would be expected if total alignment error was dominated by the measurement noise error. Thus, we have shown estimates of only the lower limits of the fish's stability.

Sex differences in the EOD

We carried out two experiments to explore sex differences in the EODs of *B. pinnicaudatus*. In the first, we digitized the nocturnal EODs of reproductive *B. pinnicaudatus* (seven males and three females) at the height of the South Florida rainy season. We set up a 115-liter tank (95 × 35 × 40 cm) adjacent to the outdoor breeding pools. Tank water, obtained from several breeding pools, was ~28 °C and ~80 μS cm^{-1} at the time of measurement. Beginning about 3 h after dark, we netted fish one at a time from their pools and allowed them to hide in a tuft of filter floss in a restraining net in the center of the tank, 1 cm below the water surface. To minimize disturbance, we lit the apparatus with a dim flashlight covered with a red filter. EOD digitizing was completed 5 min after a fish was removed from the breeding pool. We measured EODs with differential electrode pairs placed in three locations. Remote EODs were detected with Ag/AgCl wires placed at either end of the tank. EODs local to the head and tail were measured with a 6-mm dipole consisting of thin glass micropipettes with ~700-μm Ag/AgCl balls at the tips. Using a micropositioner, we placed the dipole in line with the body axis, so that the nearest electrode was first 10 mm beyond the tip of the tail, and subsequently 10 mm beyond the snout. Closer electrode placement caused these non-tranquilized fish to move. EODs were amplified differentially (CWE bioamplifier BMA-200) with a.c. coupling on the reference channel, d.c. coupling on the local EOD channel, and 10-kHz, 2-pole, Butterworth low-pass filtering on both. EODs were digitized simultaneously from the whole-tank dipole and from the 6-mm dipole at 50,000 samples s^{-1} per channel with 12-bit resolution (National Instruments DAQCard-700 A/D converter in notebook computer). We time-aligned local EODs from the head and tail by aligning post-hoc the synchronous whole-tank EODs. We show whole-tank EODs rescaled to the same peak-to-peak amplitude (Fig. 11) because the original amplitude units are not meaningful measured this way. Local EODs appear to original scale in mV cm^{-1}.

We also mapped skin potential of one male and one female *B. pinnicaudatus* measured during the day while the fish were sedated with (+)etomidate (Figs. 12, 13). During the day the EOD duration and amplitude are most stable, but the male's remote EOD waveform is also least different from the female's (Franchina and Stoddard 1999). We moved these fish directly from their outdoor breeding pools into the FIU lab and mapped their EODs with a rig similar to the one used in our previous mapping experiments.

Results

Effects of temperature on the EOD waveform: duration, amplitude, and rate

EOD duration of the female *B. pinnicaudatus* decreased linearly by 54 μs $°C^{-1}$ over the test range of 20–30 °C

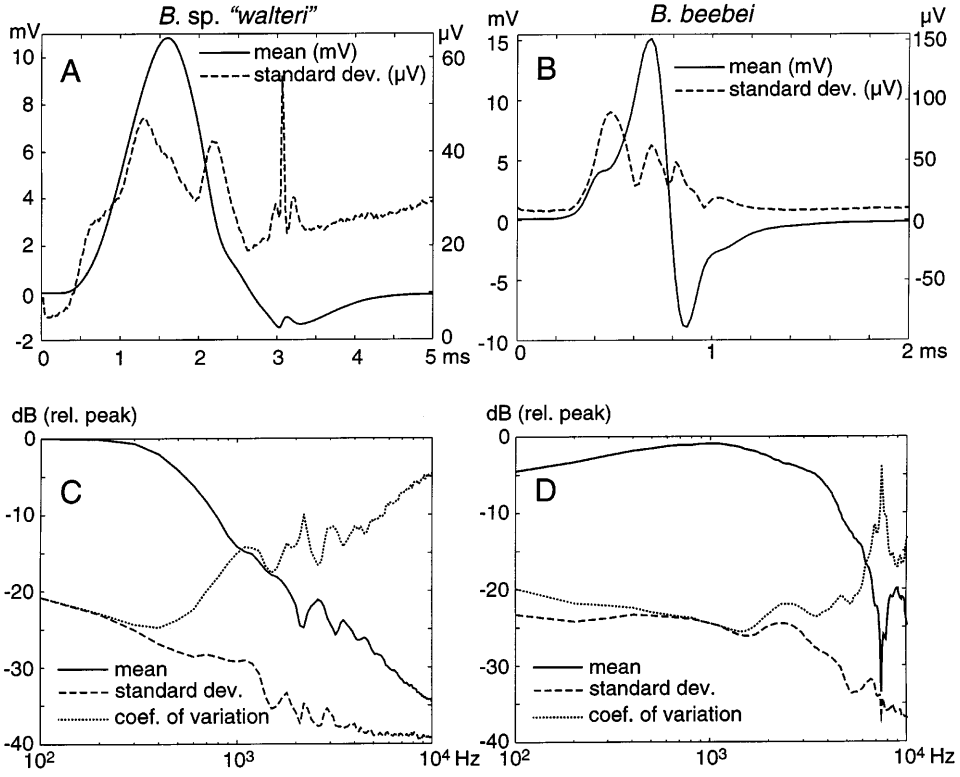

Fig. 3A–D Before we can produce maps of the electric field, we must time-align all the EODs recorded at different times and locations. We align EOD waveforms recorded on the reference stationary channel (see Materials and methods) and thus achieve temporal alignment of EODs recorded simultaneously on the movable electrodes. **A, B** Success of temporal alignment of the data is indicated by the relative magnitudes of the mean EOD recorded on the stationary reference channel (*solid line*, scaled in mV) and the standard deviation of the mean EOD (*dashed line*, scaled in μV). The standard deviation is about 1000 times smaller than the mean. The 1st phase of the EOD is less stable than the 2nd phase, perhaps because the 1st phase is produced by all the electrocytes and reflects rostro-caudal differences in spinal conduction, whereas the 2nd phase is generated by caudal electrocytes only. **C, D** Log-scaled frequency spectra of the reference channel EOD were computed by fast-Fourier transform (FFT). Frequency spectra are broad, typical of discontinuous (pulsed) EOD generation. The variance is greatest at high frequencies, beyond the dominant spectrum of the EOD

(r^2 = 0.99; Fig. 4). Durations of the 2nd EOD phase decreased slightly more than the first (P1: 22 μs $°C^{-1}$, r^2 = 0.96; P2: 32 μs $°C^{-1}$, r^2 = 0.99). A temperature change of 1 °C altered the total EOD duration by approximately 4.3%. The effect of temperature on amplitude of the 2nd phase was parabolic, peaking at 24 °C (P1: r^2 = 0.47; P2: r^2 = 0.73). At 28 °C, a temperature change of 1 °C reduced the EOD magnitude by 1.2%. The interval between EODs governed by the medullary pacemaker varied inversely with temperature. The most reasonable least-squares fit was an inverse exponential (r^2 = 0.89; Fig. 4), although the visual appearance suggests two different slopes. Except at the very high discharge rates associated with courtship signals (three to four times the normal active rate), the EOD waveform does not vary systematically with the rate of discharge (Franchina and Stoddard 1999).

Electric field components evident in the EOD waveforms

Familiar EOD time-amplitude waveforms emphasize temporal structure at the expense of spatial structure. To represent 3-D electric field vectors we plot three overlapping waveforms (rostral, dorsal, lateral Cartesian components) plus the electric potential for each point along three transects (dorsal, midplane, ventral) (Fig. 5). Visualizing 3-D electric field vectors from waveforms is difficult and we recommend readers seeking to understand the 3-D structure to focus their attentions on the other representations, in particular Figs. 7 and 8.

As would be expected of an electric dipole, the potential waveforms of the EOD at the two ends of the fish are inverted with respect to one another (Fig. 5). Waveforms at either end of the fish are not symmetrical; the 1st phase dominates the waveform near the snout (Fig. 5, 0% of body length) and the 2nd phase dominates the waveform near the tail (Fig. 5, 100% of body length). Although the EODs of most *Brachyhypopomus* species are biphasic at a distance, the autogenous EODs experienced by the fish themselves are nearly monophasic in the head region where electroreceptors are most dense. In between the head and tail, the EOD waveforms are triphasic. Comparison of the different electric field component waveforms at different points along the fishes' bodies reveals temporal disparities

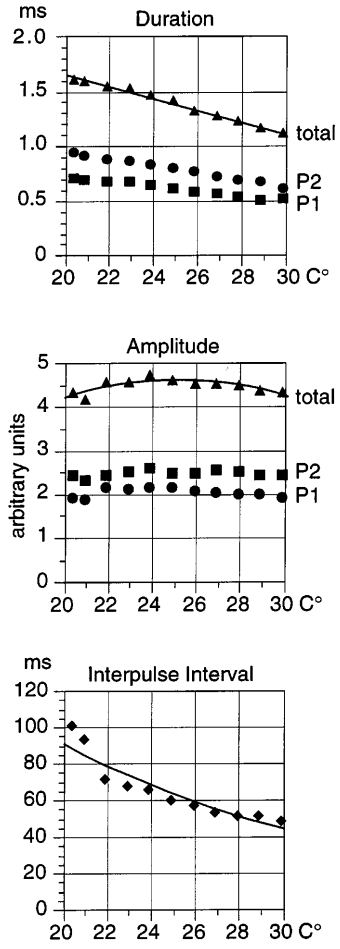

Fig. 4 Effects of temperature on the EOD of a female *B. pinnicaudatus*. EOD duration decreased linearly with temperature but EOD amplitude was affected far less. Amplitude data were best fit by an inverted parabolic curve rather than showing a simple linear relation to temperature. Discharge rate slowed significantly at low temperatures, but rate changes of this magnitude do not affect the EOD's structure

consistent with complex vector motion and intensity change. These irregularities indicate that the electric organ does not function as a simple static dipole. In fact, the dipole moves caudally during P1 (better seen in the potential maps of Fig. 6) and the vectors change considerably in their direction and intensity throughout the EOD (better seen in the vector and polar vector plots of Figs. 7 and 8). The radial electric field component is the largest in each measurement transect (dorsal, midplane, ventral) with a couple of exceptions. In both species, orthogonal rostro-caudal currents are strongest in the caudal region (Fig. 5, 70–80% of body length), indicating that the electric dipole is strongest and most stable in this region. Early in the EOD of *B. beebei* (Fig. 5, 20% of body length), a large ventrally directed current runs tangential to the skin of the midplane. This current sources (+) from the anterior dorsal trunk and sinks (−) at the anterior ventral trunk. A similar current is not seen in *B.* sp. *"walteri"*.

Maps of electric potential

False-colored movies of potential and electric field maps reveal spatial structure over an entire plane. We show selected frames from linear-weighted, pseudocolor movies in Fig. 6 and our animated color images are available over the Internet to interested readers. EOD maps, color animations, and additional software for viewing are available on our internet web sites: www.bbb.caltech.edu/ElectricFish, and www.fiu.edu/~stoddard/electricfish.html, or by anonymous ftp: ftp.bbb.caltech.edu; cd pub/ElectricFish. This paper, and not the web sites, should be cited as the source of electric field maps of *Brachyhypopomus* obtained from these online sites.

Initial activation of the electric organ in *B.* sp. *"walteri"* begins with a simple dipole field restricted to the rostral abdominal region (Fig. 6, frame 1). The region of intense positive potential is immediately caudal to the pectoral region. The dipole center remains stationary as the potential builds in intensity (Fig. 6, frame 2), but as the P1 of the remote EOD waveform approaches its peak (Fig. 6, frame 3), the dipole center has begun a smooth tailward transposition. By the time the P1 of the remote EOD wanes, the dipole center has moved to the tail where it remains stationary throughout the head-negative phase (Fig. 6, frames 5 and 6). Rostro-caudal propagation velocity of the P1 is 25 cm ms^{-1}. The P2 of the EOD is more synchronous overall than the P1. Taking local skin potential as a rough indicator of local activation of the electric organ, one can see that the anterior portion of the electric organ contributes only to the P1 of the EOD, but the posterior portion is biphasic (in the P2 the head is not actually very negative). The synchrony of the P2 produces an intense local tail positivity. While the P1 may be stronger at a distance its local asynchrony produces weaker potentials local to the fish. Differences in effective dipole length between the P1 and the P2 also contribute to the disparity between local and remote EOD magnitudes, in accordance with Coulomb's law. The larger separation between positive and negative pole centroids during the P1 should increase P1 field strength sensed at remote locations (e.g., farther than a body length) where the fish better approximates a dipole.

Potential maps of *B. beebei* (Fig. 6) show three distinct differences from those of *B.* sp. *"walteri"*. First, in *B. beebei*, initial activation of the electric organ begins closer to the head than in *B.* sp. *"walteri"* (Fig. 6, first frames). Second, in *B.* sp. *"walteri"*, the electric field dipole is oriented along the rostro-caudal axis but in *B. beebei* initial activation of the electric organ produces a dorso-ventral rotation of field dipole in which the dorsal surface is positive and the ventral surface is negative (Fig. 6, frames 1 and 2). The result of early dipole rotation in *B. beebei* is an early dorso-ventral current through the midplane (Fig. 5, 20%). Third, while in *B.* sp. *"walteri"* the tailward propagation of the dipole center is smooth, in *B. beebei*, the propagation is not smooth and the dipole fragments briefly (Fig. 6,

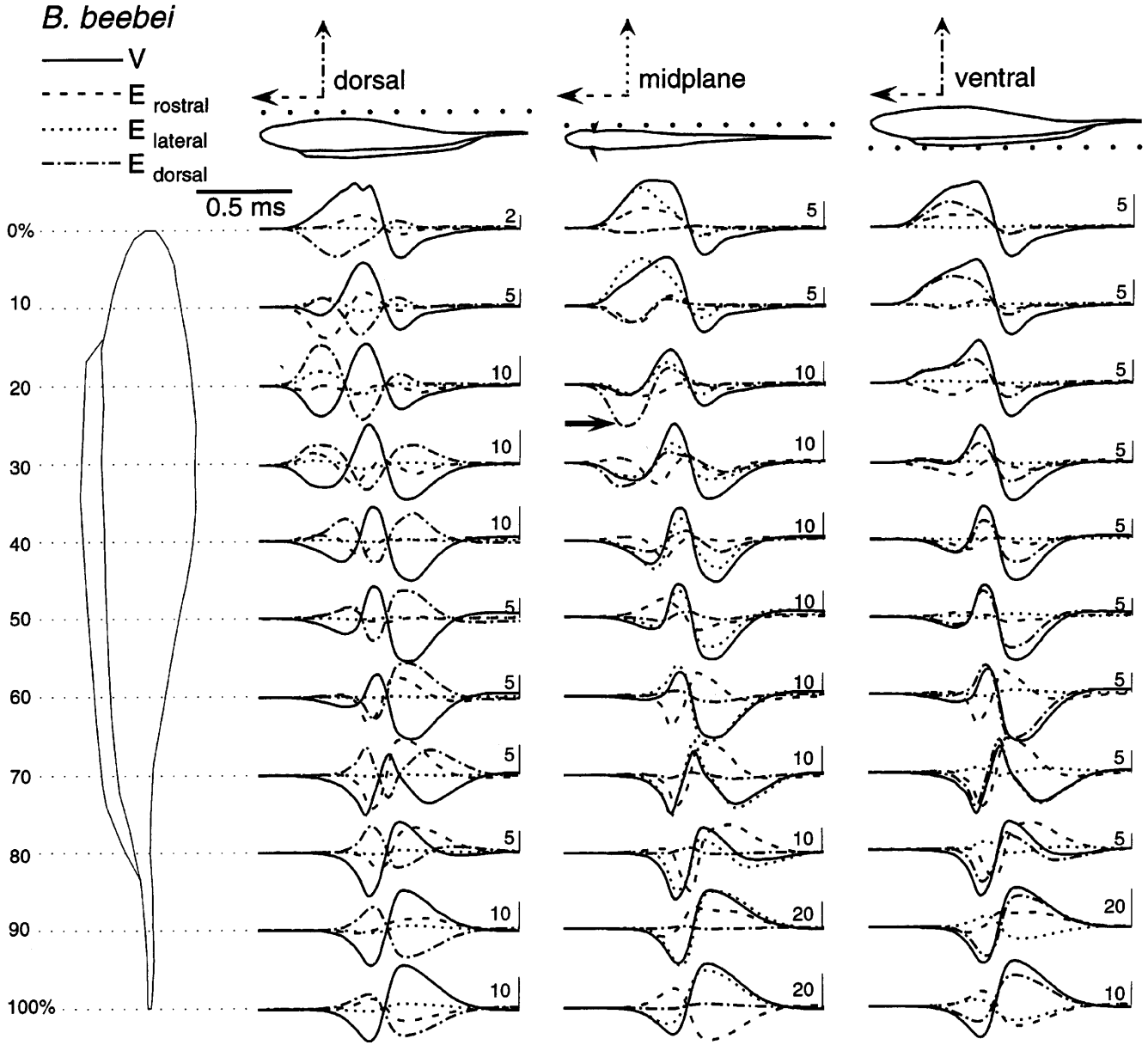

Fig. 5 Potential and electric field component waveforms of *B.* sp. *"walteri"* and *B. beebei* along three lines in the dorsal plane, midplane, and ventral plane (*top*). Waveform amplitudes have been rescaled to facilitate comparison of their shapes. The *numbers* at the right end of each waveform gives height in mV (potential) and mV cm^{-1} (field components) of the vertical scale bars next to them. An *arrow* points to a big dorso-ventral current component near the onset of the EOD of *B. beebei*

frame 2). The dipole fragments briefly again during the P1 to P2 transition (Fig. 6, frame 4). Thus, at the zero-crossing of the remote EOD, portions of the electric organ remain fully activated but the intense local currents cancel one another and are not detected at a distance. Measurements of rostro-caudal propagation velocity of the P1 are hard to interpret in this fish because the EOD is so fragmented, but the maps show a 0.135-ms latency between initial activation at the head and tail corresponding to a maximum conduction velocity of 62 cm ms^{-1}. In the potential maps from a female *B. pinnicaudatus* of comparable size (selected frames shown in Fig. 12), we measure P1 propagation of 25 cm ms^{-1}, corresponding more closely to the 29 cm ms^{-1} velocity measured by Caputi et al. (1998).

Electric field vectors

A waveform or pseudo-color map can only represent a single dimension of the 3-D electric field vector. A better sense of the directional structure of the electric field vector is seen in 2-D plots of electric field vectors. Figure 7 displays 2-D vector plots for three selected linear transects through the tank at particular phases of the EOD. The transect vector plots (Fig. 7) show extreme deviation from the field vectors expected from a simple electric dipole. Instead of a stationary dipole pattern, sources and sinks

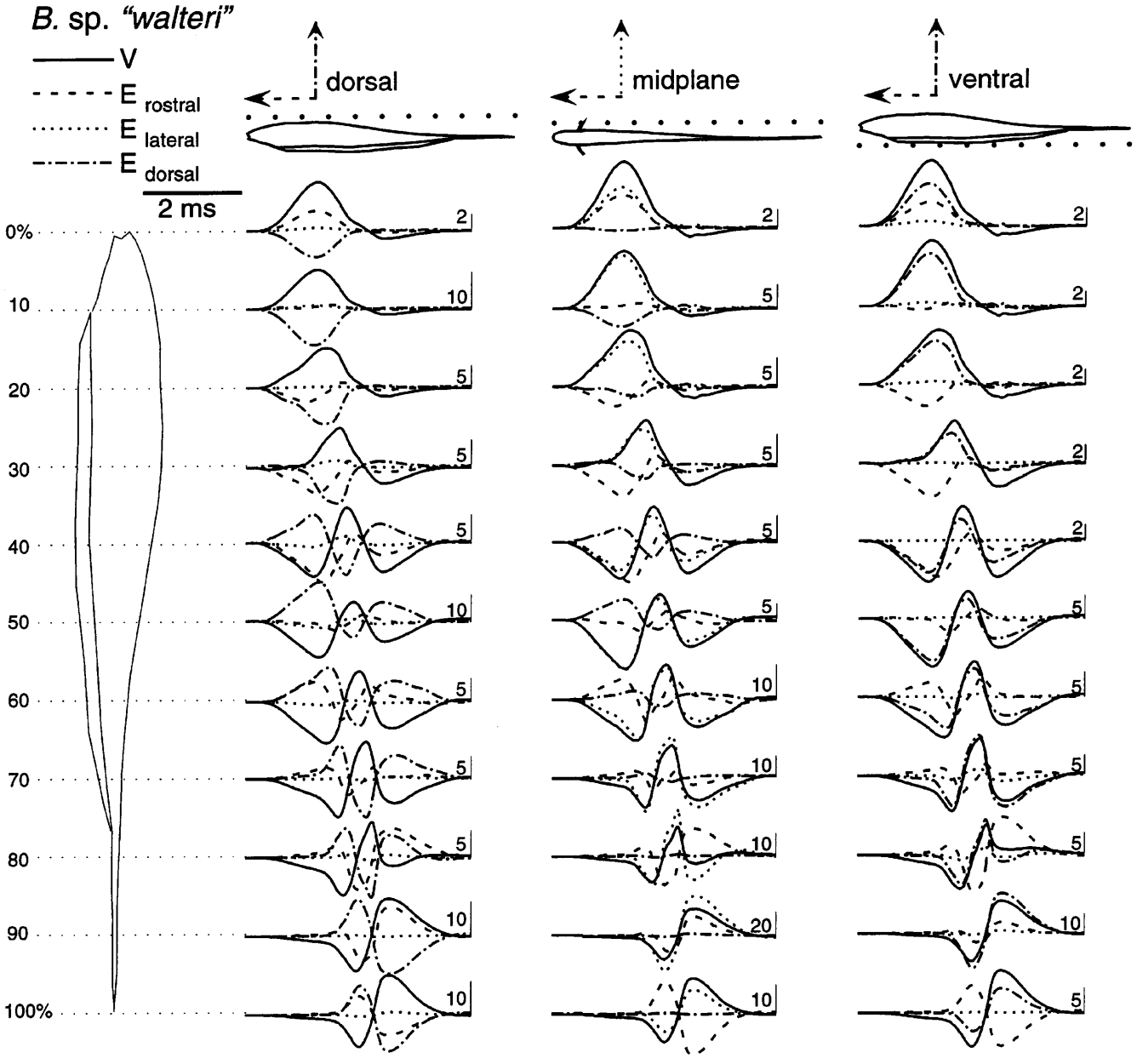

Fig. 5 (Contd)

change in size and location as excitation propagates from head to tail. Asynchrony is especially apparent in the P1. As the EOD propagates down the fish during the P1, the head region becomes quiescent. When the EOD reverses polarity, the head region is inactive. In *B.* sp. *"walteri"*, the EOD at the head is notably monophasic. In *B. beebei*, weak current flows to the head region in the P2, apparently from passive diffusion through the body. In both fish, the field is more diffuse and less intense over the anterior pole than the posterior pole, as would be expected from the roughly conical shape of the body and tail of *Brachyhypopomus*. One can infer from the bumps and twists in the contours of the field vectors (Fig. 7) that the interior of the fish is far from isopotential.

Polar vector plots (Fig. 8) give an improved representation of direction changes in the electric field vectors at selected points in three planes of measurement (dorsal, ventral, medial). Each plot represents the magnitude and direction of the electric field vector in two dimensions, at one spatial point, measured over the entire EOD duration. In the extreme head and tail regions, electric field vectors are nearly straight, oriented radially to the long axis of the body (Fig. 8). Over the rest of the body, the vectors rotate, as shown by the irregular closed loops. In *B.* sp. *"walteri"*, both peaks produce inward current at the middle of the body. If this fish were a dipole, then the current axis mid-body should be tangential to the skin, but instead the field is oriented perpendicular to the skin at both main phases. *B. beebei* appears more dipole-like, with the polar vectors arcing

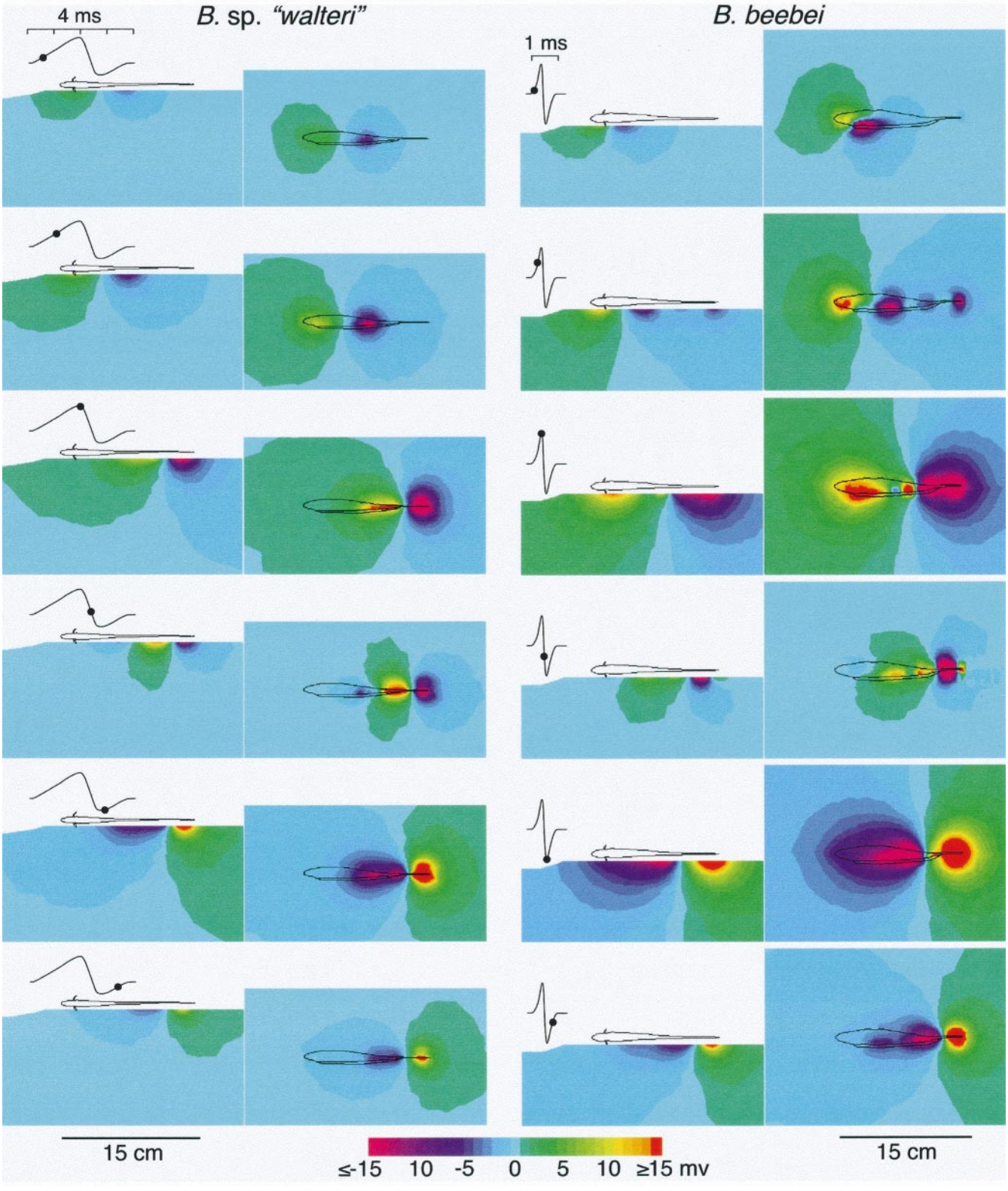

Fig. 6 Pseudo-color maps of the electric potential of *B.* sp. *"walteri"* and *B. beebei*. Potentials are shown in the lateral and dorso-ventral planes. Frames are shown at different times in the EOD indicated by *dots* on the accompanying remote EOD waveform. The surface of the fish in the maps of the dorso-ventral plane shows measurements taken directly on the skin

tangentially between mid-body and the tip of the tail. The extent of monopolarity at the head is evident in the proximity of the start and end points (thin circle) to the peak of the P2 (open dot). In *B.* sp. *"walteri"* the end points are concentric with the peak of P2, indicating complete monopolarity. The weak P2 at the head of

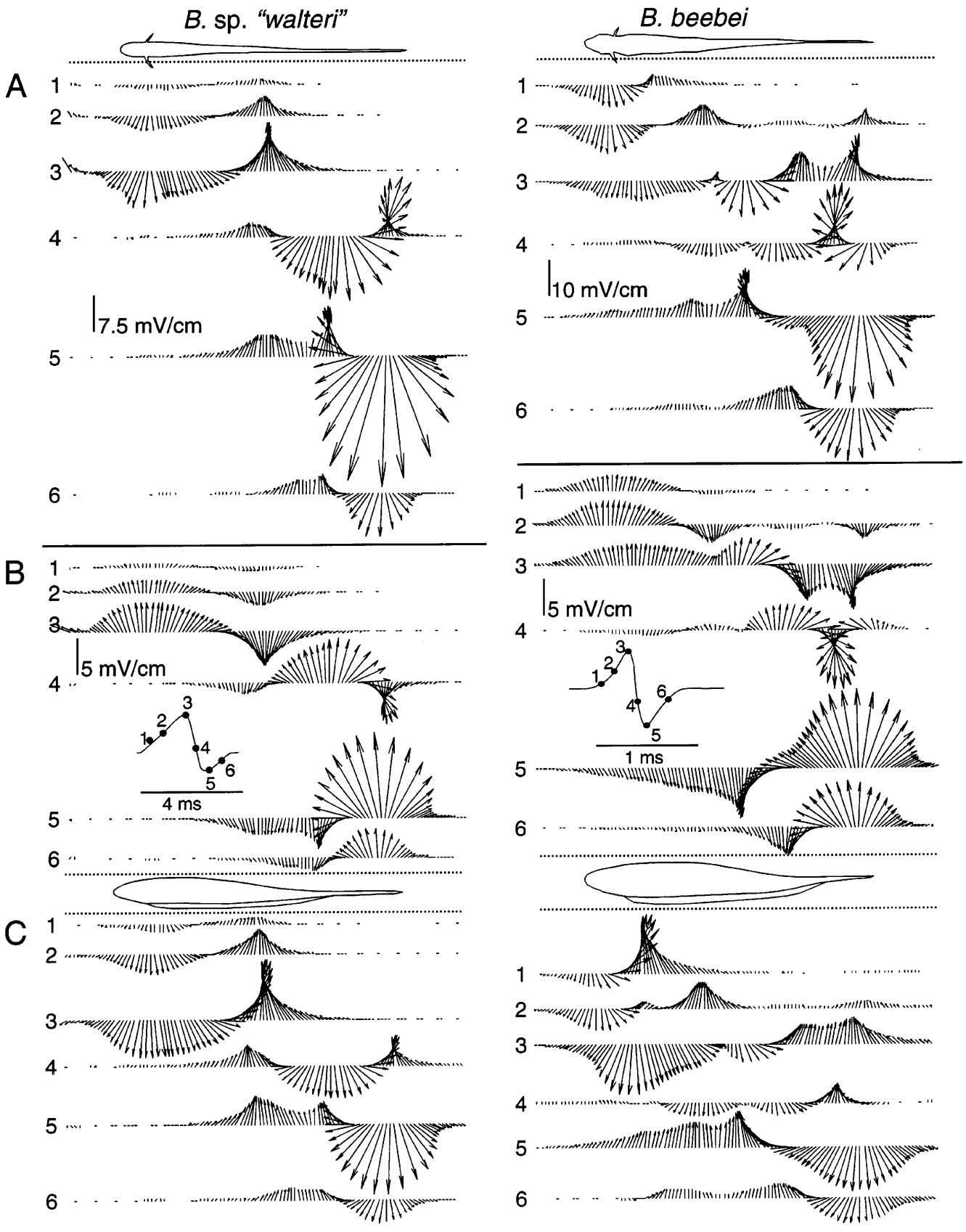
B. sp. "walteri"
B. beebei
A
B
C
1
2
3
4
5
6
7.5 mV/cm
10 mV/cm
5 mV/cm
4 ms
1 ms

◄

Fig. 7A–C Transect vector plots of the EOD of *B.* sp. *"walteri"* and *B. beebei*. Each plot shows two of the three Cartesian components of the electric field vectors along three transects, immediately lateral (**A**), dorsal (**B**), and ventral (**C**) to the fish. Each transect is shown at six phases of the EOD. *Numbers* to the left of each vector row correspond to the phases marked on the accompanying EOD waveform. Intensity in each vector row is shown relative to the vertical scale bar

B. beebei is evident from the slight offset between the 2nd peak and the endpoint marks.

EOD amplitude lateral to the body and lateral attenuation

The intensity of the electric field vectors shown in each of these plots changes spatially over orders of magnitude. We have rescaled our plots to facilitate comparison between different points in space. To give a better sense of absolute intensity, we plot peak-to-peak magnitudes of the electric potential and field of entire EODs along transects lateral to the body (Fig. 9), plus the exponents of the attenuation slopes of those curves. We present measurements of peak-to-peak electric field magnitude which may best describe the parameter that excites tuberous electroreceptors.

The peak-to-peak potential of the long duration EOD species, *B.* sp. *"walteri"*, was weaker than that of short duration EOD species, *B. beebei* (Fig. 9). One centimeter from the body, the peak-to-peak potential ranged from about 8 to 20 mV in *B.* sp. *"walteri"* and 18–50 mV in *B. beebei*, about 2-2.5 times stronger. In both species, amplitudes 1 cm lateral to the tail were 2–2.5 times stronger than 1 cm lateral to the head. Potential in *B. beebei* 10 cm lateral to the point 3/4 along the body length was an order of magnitude weaker than 10 cm lateral to the head or tail. This dip in potential strength corresponds to an approximation of the zero-potential plane that would be found lateral to the midpoint of a true dipole. That this potential dip is not seen in the potential of *B.* sp. *"walteri"* is a consequence of the smooth caudal propagation of the head-positive phase of the EOD in that species. Peak-to-peak electric field magnitudes differ qualitatively from potentials. In *B.* sp. *"walteri"* the four tracks converge as we measure increasingly lateral to the body, the field magnitudes becoming spatially uniform 4 cm lateral to the body. In *B. beebei*, field magnitudes at the head and tail converge around 11 cm lateral to the body, but field magnitudes 3/4 along the body length depart from the other values, diminishing at a greater rate as distance increases.

In the water around the fish, the electric potential and field do not attenuate with distance at a constant slope (Fig. 9). In both species, the potential attenuates less steeply than r^{-1} within 1 cm of the body, approaching about $r^{-1.5}$ more laterally. The electric field of *B.* sp. *"walteri"* dropped off with an exponent of −1 within 1 cm of the head and approached −1.5 to −2 more laterally. The attenuation slope of the electric field of *B. beebei* ranged from −1.5 to −2 over the entire measurement range. In general, the slope is shallower closer to the head where the body is thicker and the local sources resemble a surface charge (exponent zero). The slope is steeper close to the tail because the localized charge within the thin caudal filament better resembles a point charge (exponent −2). Note that the exponent of the attenuation slope depends critically on the choice of origin. We chose the body midline for the origin of the distance scale because it forms the field's axis of symmetry.

Direct current imbalance

The direct current (d.c.) component of the EOD should influence detectability by the ampullary systems of predators and conspecifics alike (Stoddard 1994; Stoddard et al. 1995). The d.c. component results from asymmetry in the *time* × *voltage* integrals above and below the 0-V baseline. In Fig. 10 we compare the rms of the electric field to the d.c. component of the electric field vector, calculated as the rms of the positive portion minus rms of the negative portion. Close to the body (~1 cm lateral) the d.c. value of the electric field is about one-third of the total electric field magnitude (Fig. 10). Seven centimeters lateral to the body, d.c. differs pronouncedly between the tail and the rest of the fish in both species: in *B.* sp. *"walteri"* d.c. lateral to the tail is 20–30% that lateral to other parts of the body; in *B. beebei* the difference is smaller, 30–60%. At the lateral extent of our measurements (13 cm, almost a body length), d.c. is 30–60% of total electric field magnitude in *B.* sp. *"walteri"*, but only 10–20% of total electric field magnitude in *B. beebei*. Even though total electric field magnitude of *B.* sp. *"walteri"* is about half that of *B. beebei*, the d.c. component is of similar magnitude for the two species, 14–30 μV in *B.* sp. *"walteri"* and 10–20 μV cm^{-1} in *B. beebei*.

Sex differences in waveforms

B. pinnicaudatus are known for the sexual dimorphism of their caudal filaments and their EODs (Hopkins et al. 1990; Hopkins 1991; Franchina and Stoddard 1999). We digitized the EODs of seven males and three females at night in a large tank adjacent to their breeding pools. Figure 11 shows axial electric field waveforms of a representative male and female measured at night around the time of maximum sexual dimorphism in the EOD. Waveforms are shown time-aligned to the peaks of the head-positive phases of the EODs measured at the tank walls (see Materials and methods). Figures 12 and 13 show electric potential measured during the day in a pair of lightly tranquilized fish. Waveform measurements in Fig. 13 are from points overlying the electric organ. A question arises how to compare points along the bodies of mature males and females, because the sexes have

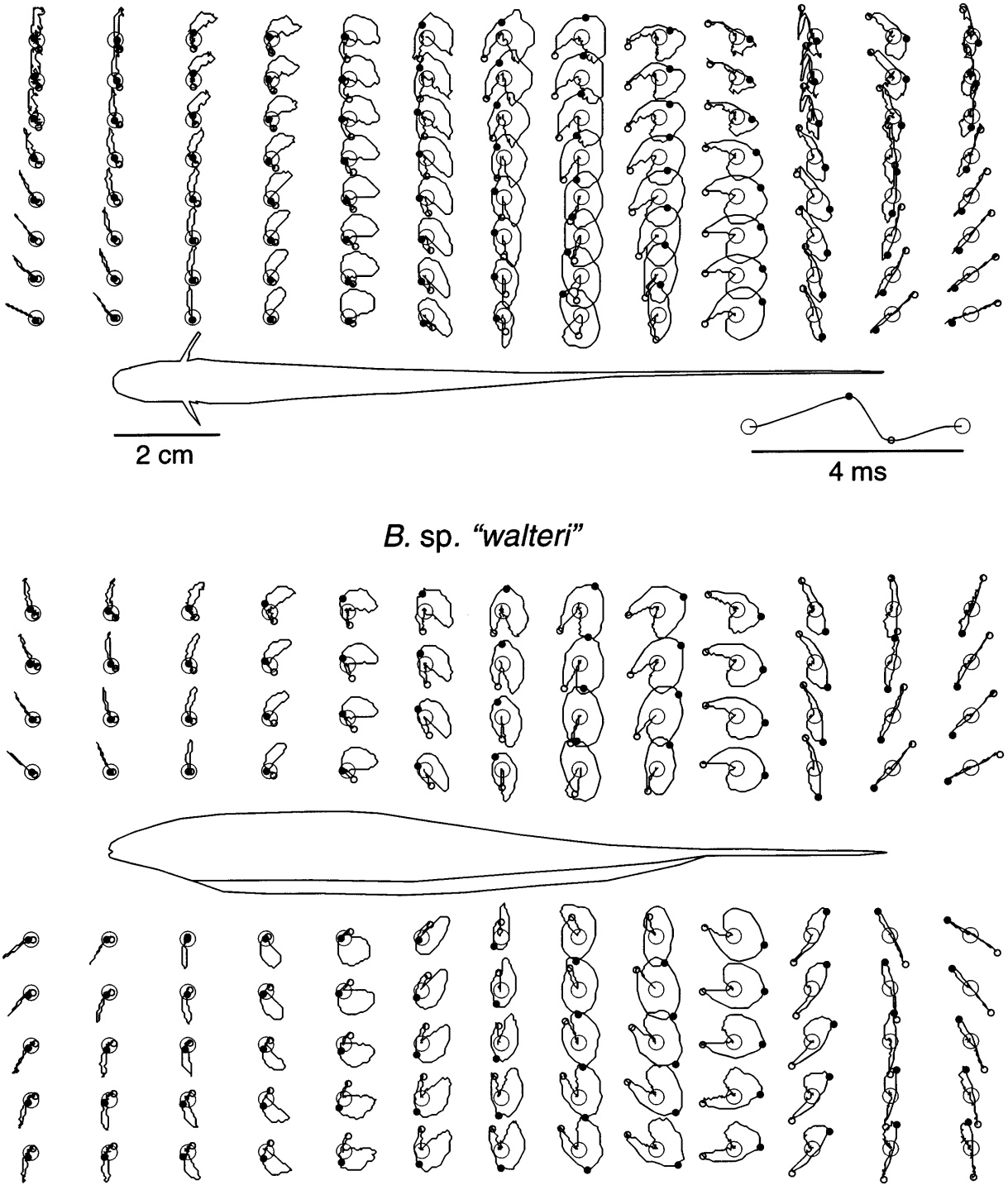

Fig. 8 Polar vector plots of the EOD of *B.* sp. *"walteri"* and *B. beebei* shown every 10% of the fish's length and at several distances lateral, dorsal, and ventral to the fish. Each squiggle depicts the magnitude and planar direction across an entire EOD. Four points in time are marked in each squiggle: *thin-lined open circles* mark the beginning and end points at 0 mV cm^{-1}, the *black circle* marks the peak of P1 measured near the tail, and the *open circle* marks the peak of P2 measured near the tail. EOD peaks are indicated for the EOD measured near the tail where the magnitude is greatest. Further anterior, the small dots *do not* indicate the local EOD peaks because the anterior regions of the electric organ are activated earlier than those at the tail. The roundness of the plots indicates the degree of rotation of the electric field vectors in the other regions around the fish's body. Thus, the linearity of the vector plots at and beyond the head and the tip of the tail indicates that the electric field vectors are nearly unidirectional in these regions. Each squiggle is normalized to have the same maximal radius; thus, points far from the fish contain more measurement noise

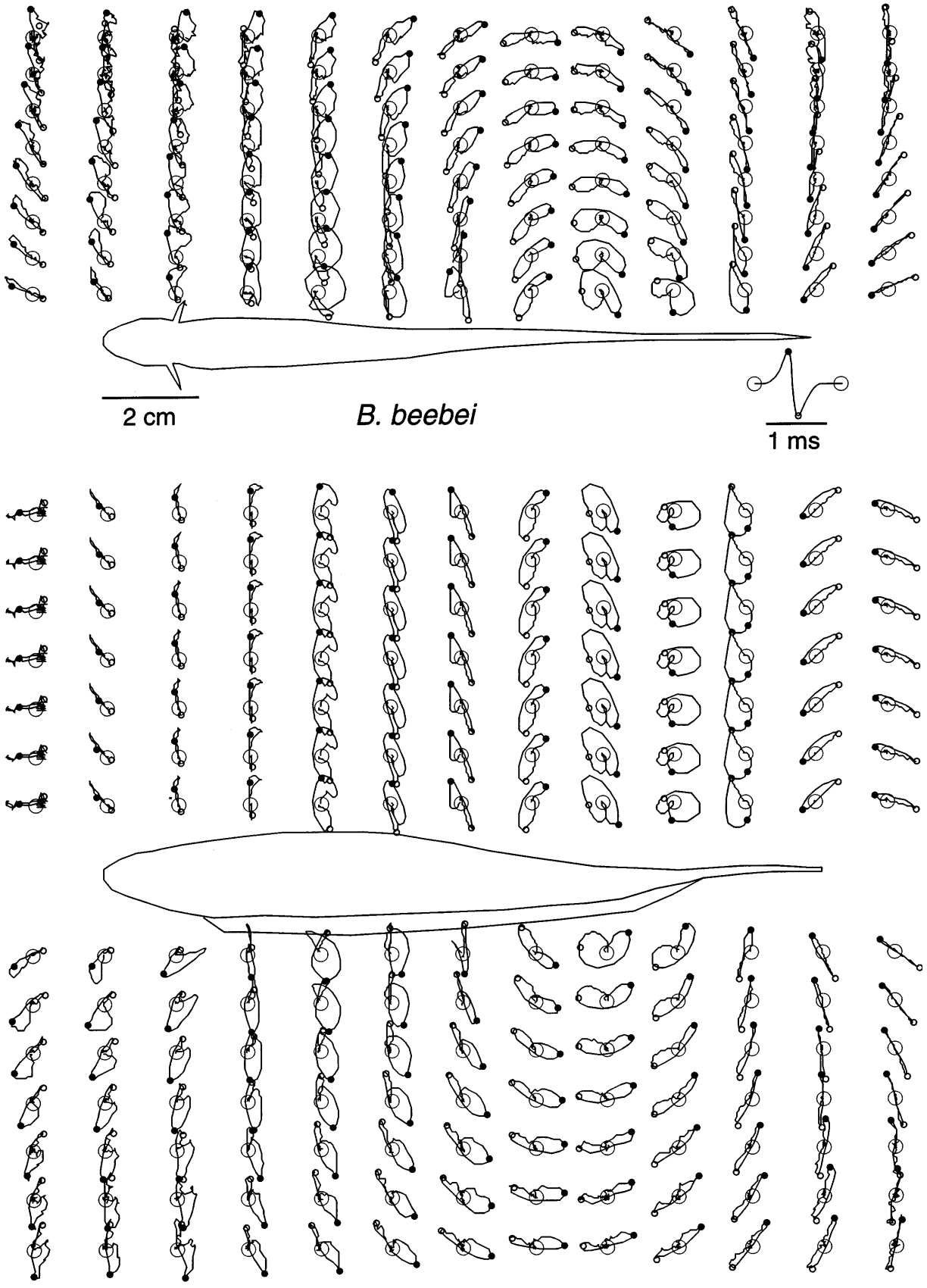

Fig. 8 (Contd)

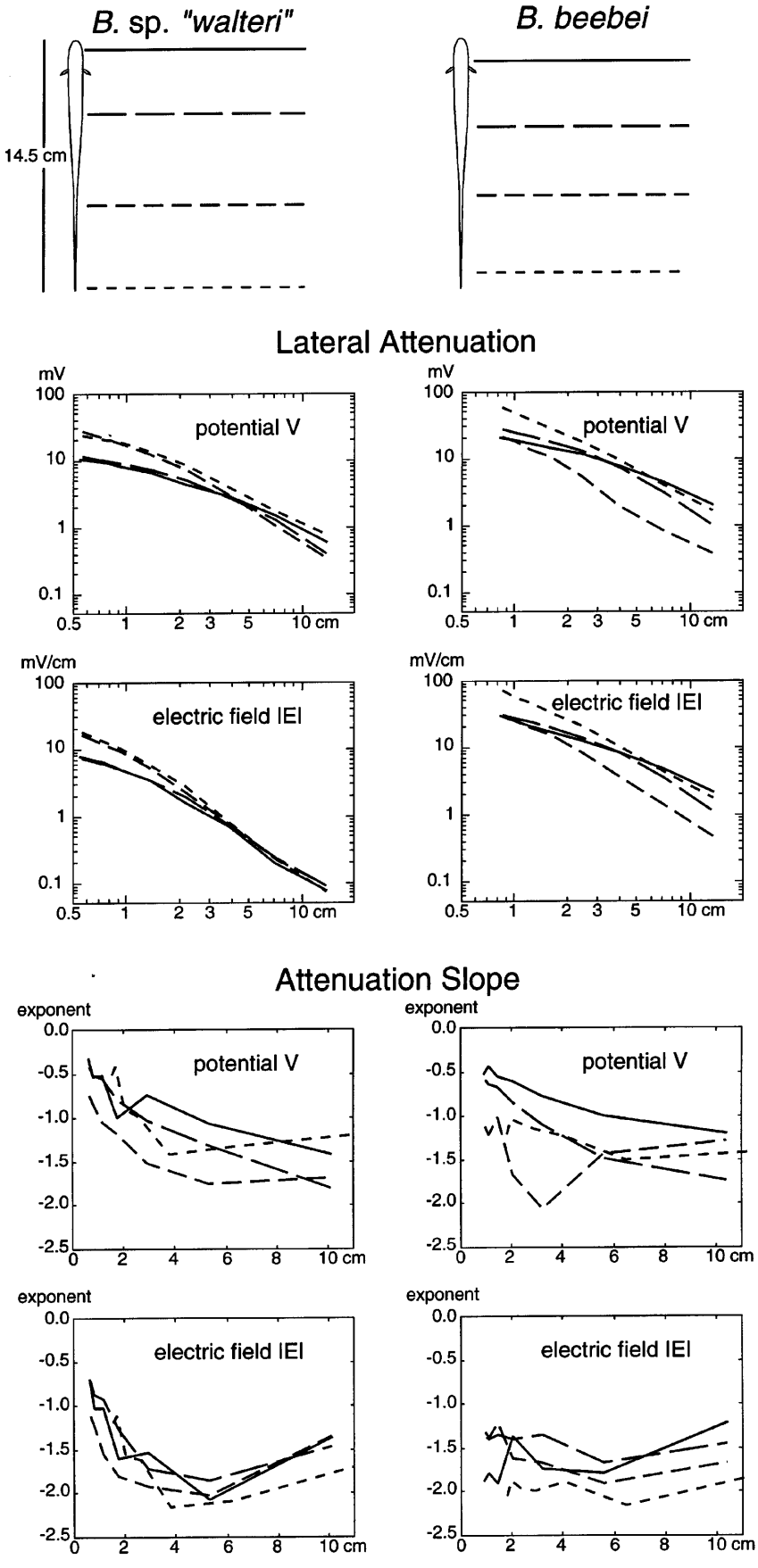

Fig. 9 Peak-to-peak potential and electric field magnitudes mapped along four transects lateral to 14.5-cm female *B. beebei* and *B.* sp. *"walteri"*. The EOD of *B. beebei* is stronger than that of *B.* sp. *"walteri"*. Details are described in the text. Attenuation slopes are calculated from the same measurements shown in Fig. 8. The potential attenuates less steeply than r^{-1} within 1 cm of the body, approaching about $r^{-1.5}$ more laterally. The electric field of *B.* sp. *"walteri"* dropped off with an exponent of −1 within 1 cm of the head and approached −1.5 to −2 more laterally. The attenuation slope of the electric field of *B. beebei* ranged from −1.5 to −2 over the entire measurement range

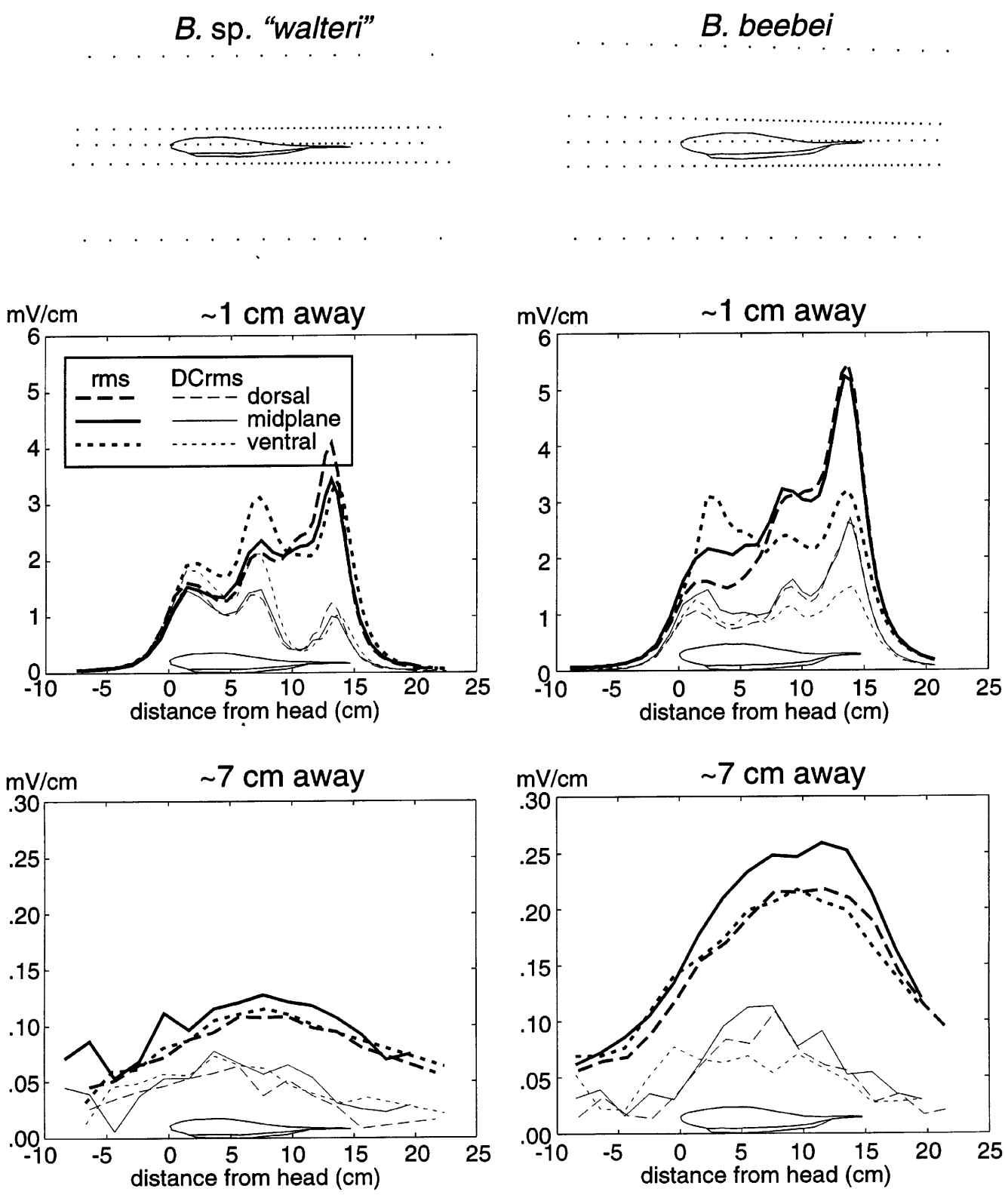

Fig. 10 Root mean square (rms) and d.c. rms components of the electric field are calculated here along different transects parallel to the fish, ~1 cm away and ~7 cm away from the body. Measurement points are shown at the top of the figure with points along the midline extending out of the paper a distance similar to the displacement of the dorsal and ventral tracks. d.c. rms is calculated as the rms of the positive values minus the rms of the negative values. In the ~1-cm transects, the d.c. rms is nearly equivalent to the rms because local EODs are so imbalanced with respect to 0 V. Farther from the fish, (e.g., the ~7-cm transects) the waveforms become more symmetric and the fraction of d.c. rms declines relative to rms. The zig-zags in the ~7-cm plots result from measurements near the noise floor of the digitizing system

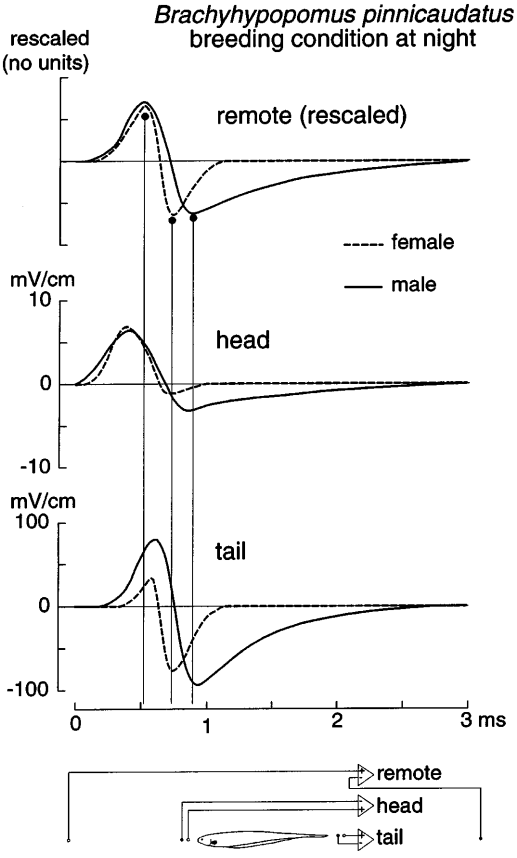

Fig. 11 Sexual dimorphism is shown by EOD waveforms of representative captive bred *B. pinnicaudatus* in reproductive condition. The fish were measured several hours into the night when sexual dimorphism in the EOD is greatest. The schematic below shows the geometry of the measurement system. Details are described in Materials and methods. EODs measured remotely (head-tail) are rescaled to the same peak-to-peak height to facilitate comparison of the shapes of the waveforms (this male's remote EOD is about three times larger than the female's). EODs measured near the head and tail are plotted without rescaling so amplitudes may be compared as well. Note the similarity of the EOD waveforms measured near the head in contrast to those measured near the tail. *Vertical lines* facilitate comparison of the timing of the waveform peaks and show that the head EOD leads the remote EOD by about 200 μs and the tail EOD lags it by a lesser delay. The peak of the 2nd phase at the tail is synchronous with that measured remotely

very different body shapes. Hopkins et al. (1990) addressed this problem by considering both total body length and length from the snout to the caudal end of the anal fin (LEA). In Fig. 13 we scale the two fish to the same LEA. Even thus scaled, ignoring the sexually dimorphic caudal filament beyond the anal fin, one can see that the male's body is proportionally thinner than the female's.

Durations

Remote EOD waveforms show the extended P2 characteristic of the male's EOD (Fig. 11). The P1 of the male EOD is about 20% longer in the male, as seen in the offset zero crossings. The P2 is three to four times longer in the male than the female, depending how close to the baseline one measures. One centimeter rostral to the head, durations of P1 are slightly greater in the male, and the slopes of this phase are more gradual. The duration of the P2 of the female near the head is about half that of the P1; in contrast the P2 of the male is about three times that of the P1. The P1s of both sexes peak about 120 μs earlier near the head than in the remote EOD (see vertical lines in Fig. 11). One centimeter caudal to the tail, the female's EOD seems almost an amplified reverse image of the EOD measured near the head; the female's P2 is about twice as long as the P1. The male's EOD at this location more closely resembles the remote EOD and differs mainly in that it occurs with an appreciable delay (see vertical lines in Fig. 11). The P1 of both sexes peaks about 200 μs later at the tail than at the head.

Amplitudes

In EODs measured 1 cm rostral to the head, the amplitude of the P1 is similar for the male and female but the amplitude of the P2 is about three times greater in the male. In EODs measured 1 cm caudal to the tail, P1 is about twice as large in the male as the female but the male's P2 is only 20% larger than the female's. P1s at the tail are ten times and five times larger than P1s at the head in males and females, respectively.

Skin maps of *B. pinnicaudatus* (Fig. 12) are very similar to those of its sister species *B. beebei*, the only major difference being that the duration is about 50% longer. Skin maps of the two sexes are likewise extremely similar to each other in spite of the striking sexual dimorphism in the length and thickness of the caudal filament. As the P1 of the male's remote EOD reaches its peak, a stationary positive pole appears at about 60% of body length (Fig. 12, row 3). As the P1 wanes, this pole begins to propagate caudally, continuing as the dipole fragments into five poles at the zero crossing (Fig. 12, row 4). At the peak of P2, the poles have coalesced into a head-negative dipole. At the two peaks of the remote EOD, the caudal filament is monopolar, entirely positive in P1 and entirely negative in P2. However, the zero-potential plane of the dipole is not the same at these two peaks. The zero-potential plane is more anterior at the peak of P1 than at the peak of P2.

As expected, potential waveforms (Fig. 13) are less sexually dimorphic during the day than at night. Fig. 13 shows another sex difference; waveforms at the midbody differ between the sexes, as noted by Caputi et al. (1998). The female's EOD shows an early inward current from 3 cm on back to the tip of the tail, diminishing between 8 and 9 cm. From 10 cm to the tip of the tail is a delayed inward current. The male likewise shows similar inward currents from 3 cm on back; however, between 11 and 12 cm early currents are absent, rendering these local EODs head-positive biphasic instead

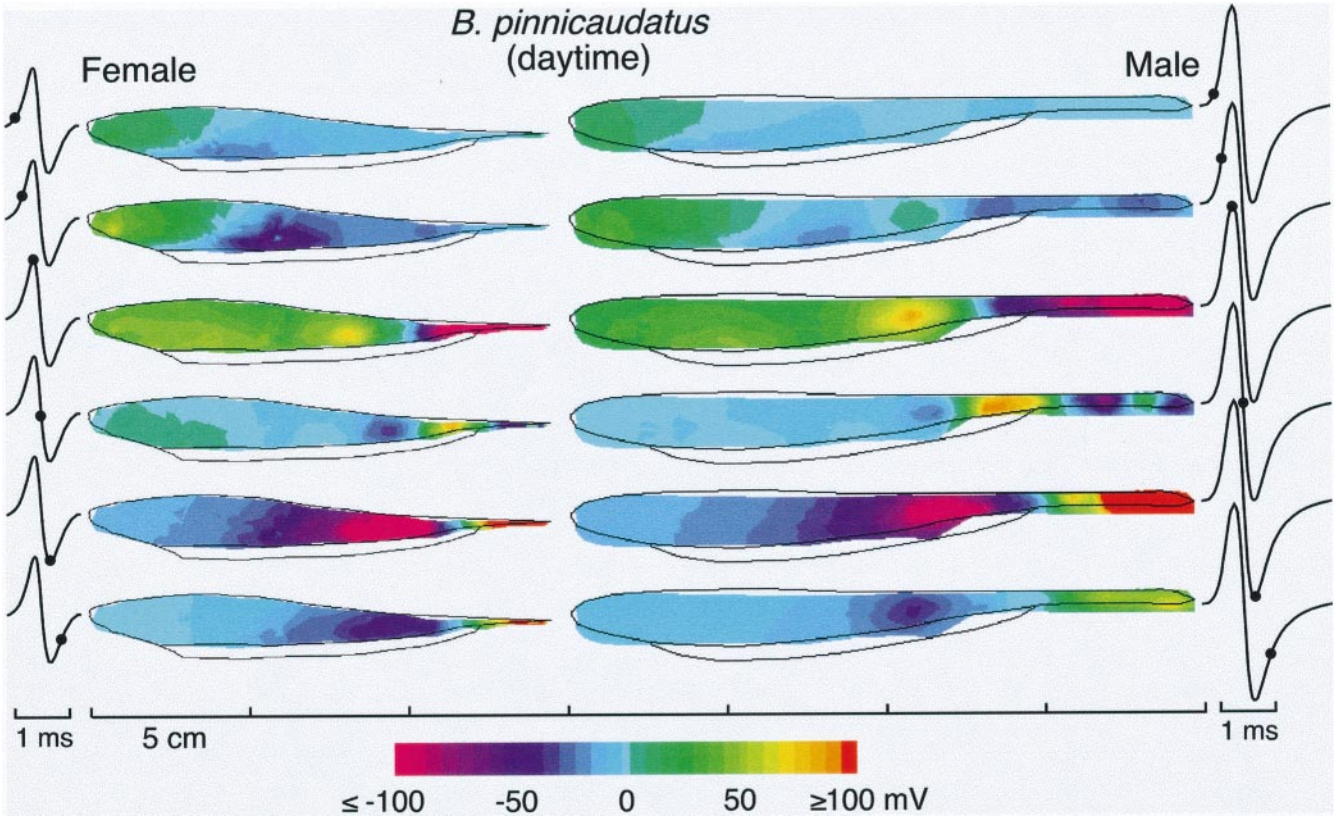

Fig. 12 Pseudo-color maps of electric potential of reproductive male and female *B. pinnicaudatus* measured on the skin during the daytime when sexual dimorphism is at its minimum and EODs are most stable. Other details are as with the potential maps shown previously. At the amplitude scales shown here, little qualitative difference is evident between the potential maps of the two sexes except for the gross sexual dimorphism in tail morphology

of triphasic as in the female. In both sexes, the early inward current just anterior of 3 cm reflects the sinking of the early head-positive outward current local to the anterior extent of the electric organ around 2 cm. The absence of the inward current from the 11- to 12-cm region of the male's body is due to his lengthened electric organ. In the female, the anterior dipole sink is continuous with the caudal dipole source, whereas in the male, anterior sink and caudal source are separated by a couple of centimeters.

Discussion

Temperature effects

The strong effect of temperature on EOD duration emphasizes the importance of stable temperature during our 4-h EOD mapping sessions. That both phases contributed to the decrease in EOD duration with increasing temperature suggests that ion channel thermokinetics are responsible for the temperature effect on EOD duration. As water temperature rises during the day and declines at night, EOD duration should likewise shorten and lengthen. EODs of *B. pinnicaudatus* do change measurably between day and night, but the EOD changes lead temperature changes in phase by several hours and greatly exceed the change one would expect from temperature alone (Franchina and Stoddard 1999). Caputi et al. (1998) found that the 2nd phase of the EOD fails (i.e., disappears) when sexually immature *B. pinnicaudatus* are brought indoors from the cool winter waters of Uruguay and measured in water at 30 °C. The fish we used in our temperature trial were also tested during the winter but we saw no failure of the P2. In fact, the change in P2 amplitude tracked closely the change in P1 amplitude (Fig. 4). The main methodological difference between our result and that of Caputi et al. (1998) was that our subjects were sexually mature females, whereas theirs were "non-differentiated" fish of unknown sex, i.e., grown, but sexually immature. Both populations originated in similar subtropical regions (Argentina and Uruguay). Caputi et al. (1998) did not see similar EOD changes in the summer when fish were sexually differentiated, and speculate that hormones may interact with electrocyte membranes to adapt the electric organ to changes in temperature. Our findings add further support to their hypothesis.

Dipole separation

Coulomb's law shows that electric field strength of a distant dipole is linearly proportional to the distance

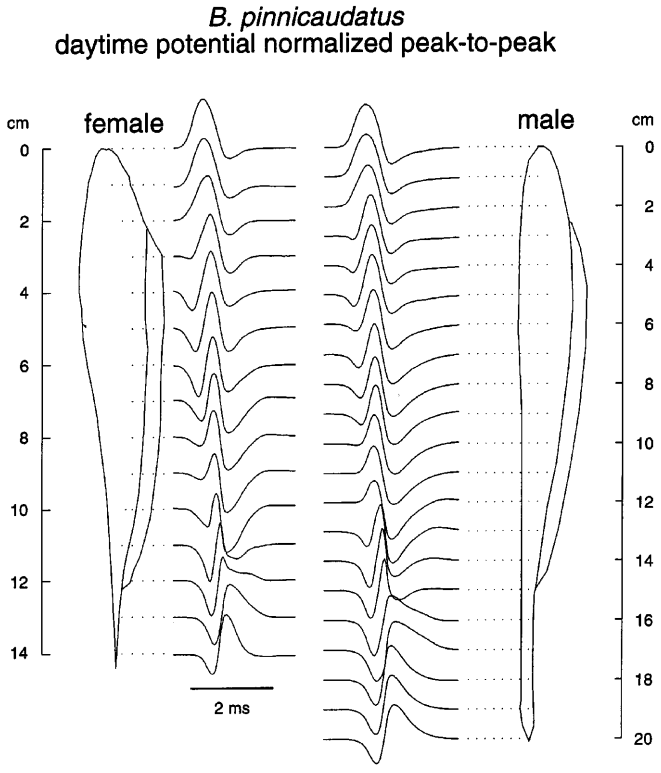

Fig. 13 Sex differences in daytime potential waveforms plotted from the same data set as shown in Fig. 12. Selected points overly the electric organ. The two fish are scaled here to equate length to end of anal fin. Note the sex difference midbody where the male's EOD becomes purely biphasic. An explanation is provided in the text

between the poles. Thus, a mechanism for increasing electric field strength is to increase separation between the positive and negative poles by insulating the columns of electrocytes so that current can only escape the electric organ from its ends. The membranes surrounding the electrocyte columns can be highly resistive (Bennett 1971), but judging from the broad areas of activation evident in our skin maps of electric potential, these membranes must be somewhat conductive in *Brachyhypopomus*. Visual inspection of the potential maps and the transect vector plots (Figs. 6, 7, 12) shows that the effective dipole separation is only about one-third of total body length. One trend is apparent: the broad activation of the electric organ during the head positive phase produces a greater effective dipole separation during P1 than during P2. So, even though the local field intensity is greater during P2 (Figs. 7, 10) the shorter dipole separation reduces the relative magnitude of the P2 in the waveform measured remotely (Figs. 1, 10).

Mechanism of EOD spatial heterogeneity and motion

The EODs of the biphasic *Brachyhypopomus* species are spatially heterogeneous, and temporally fractured and mobile. This complexity contrasts sharply with the EOD of *Eigenmannia* sp. (Gymnotiformes, Eigenmanniidae), which resembles a simple electric dipole (Assad et al. 1998). The electric field vectors over the body surface of *Eigenmannia* radiate as would be expected for a dipole within a fish body, and the dipole center remains stationary throughout the EOD. Comparative mapping results allow us to infer differences in spatial organization and synchrony of the electrocytes throughout the electric organ working as a whole. We postulate that four distinct factors contribute to the temporal and spatial heterogeneity of the EODs of *Brachyhypopomus* spp.: spinal conduction, leaky insulation of the electric organ, heterogeneous conduction within body tissues, and differences between anterior and posterior electrocytes.

First, to produce the rostro-caudal propagation of the dipole center seen in the skin potential maps and vector plots described above, electrocytes must activate asynchronously, starting with the anterior electrocytes closest to the medullary pacemaker nucleus. The smooth rostrocaudal propagation of the EOD of *B.* sp. *"walteri"* suggests a lack of pathlength compensation in conduction of the spinal command pulse down the spinal column of the sort found in the gymnotiform genera *Electrophorus*, *Eigenmannia*, and *Gymnotus* (Albe-Fessard and Martins-Ferreira 1953; Bennett 1971; Lorenzo et al. 1990; Assad et al. 1998). In these other species, axons innervating the caudal electrocytes are larger in diameter than those innervating the rostral electrocytes and they take a more direct route (Bennett 1971). The slow (25 cm ms^{-1}) rostrocaudal propagation of the EOD of *B.* sp. *"walteri"* falls towards the low end of reported conduction velocities (Lorenzo et al. 1990). We and Caputi et al. (1998) report insignificantly higher conduction velocities of 26–29 cm ms^{-1} for female *B. pinnicaudatus* which produce an EOD less than half as long, but the shorter EODs of *B. pinnicaudatus* (and *B. beebei*) are accompanied by a spatial skip in the rostro-caudal transition wherein the caudal filament becomes active before the more anterior regions are quiescent. This skip results in a fractionation of the dipole into four distinct poles measurable on and near the skin. Assuming the pacemaker and relay neurons are synchronized in these fish (Spiro 1997), the spatial break in the brief EODs of *B. pinnicaudatus* and *B. beebei* may involve partial pathlength compensation in the spinal command axons. The faster P1 conduction measured in *B. beebei* (62 cm ms^{-1}) is consistent with this interpretation. Sullivan's (1997) phylogeny of the Hypopomidae indicates that the long EOD of *B.* sp. *"walteri"* is derived from ancestors with shorter EODs. The long-duration waveforms of *B.* sp. *"walteri"* result both from long-duration activation of local sinks and sources and rostro-caudal propagation of the region of activity that spreads the remote waveform in time. Electrocyte ion channel kinetics may be involved as well (Ferrari et al. 1995).

The second mechanism promoting spatio-temporal heterogeneity of the electric field is partial insulation of the electrocyte tubes. Insulation creates functional electrogenic units considerably longer than a single

electrocyte (Bennett 1971). Insulating membranes surrounding the electrocyte columns must be significantly leaky, however, or the dipole center and spatial extent of activation would remain stationary on the skin in spite of rostro-caudal propagation of activation within the electric organ (see also Caputi et al. 1989).

Third, heterogeneity of body resistivity must result in spatial heterogeneity of potential and field lines on the body surface. In the potential maps of *B. beebei* (Fig. 6) the dipole axis is tilted from the horizontal at the onset of the EOD, resulting in a large dorso-ventral current (Fig. 5, 20% of body length). The electric organ of *B. beebei* begins just posterior to the operculum, anterior of the swim bladder. In addition to regulating buoyancy, the air in the swim bladder functions as an insulating structure, dividing the conductive tissues of the trunk dorso-ventrally. Initial positive charge from early activation of the rostral electrocytes is probably diverted dorsally by the swim bladder resulting in the observed tilt of the dipole. Initial source and sinks on the skin of *B.* sp. *"walteri"* are located more caudally than those of *B. beebei*, so initial activation should not leak around the rostral end of the swimbladder to the same degree. This difference may account for the more uniform geometry of the initial dipole in *B.* sp. *"walteri"*. Were the body interior truly isopotential, as is sometimes assumed, neither the dorso-ventral position of the horizontally oriented electric organ nor its rostral extent would produce dorso-ventral currents at the skin. Thus, we conclude that the passive resistive properties of the body interior are heterogeneous and substantially modify the current pattern from the electric organ.

A rostro-caudal difference in electrocyte physiology is the fourth mechanism promoting spatio-temporal heterogeneity in the electric fields. The potential maps show that the electric organ throughout the length of the fish contributes to the head-positive phase of the EOD, but only the posterior half of the electric organ appears active during the head-negative phase. Differences between rostral and caudal electrocytes must therefore contribute significantly to spatial heterogeneity in waveform. Bennett (1961, 1971) found that all electrocytes in *Brachyhypopomus* spp. fire on their posterior, innervated faces, producing the head-positive phase of the EOD waveform, but that in species with a biphasic EOD, electrocytes in the caudal third of the electric organ also fire on their anterior, non-innervated faces as well, producing the head-negative phase of the EOD. By examining the motion of sources and sinks in the skin maps, we can see that the head-positive phase moves rostrocaudally but the head-negative phase is nearly stationary and synchronous. Thus, we infer that the anterior, non-innervated faces of posterior electrocytes of *Brachyhypopomus* spp. fire nearly simultaneously in contrast to the posterior innervated faces that depend on spinal conduction and cholinergic activation.

Although the fine structure of the local electric field degrades sharply with distance, fragmentation of the local EOD does affect the remote, composite EOD. The uneven rostro-caudal propagation of the head-positive phase of the EOD seen in *B. beebei* and *B. pinnicaudatus* can produce multiple local peaks that are offset in time. Spatial summation of these peaks at a distance results frequently in bumps in the rising slope of the first phase (e.g., mean mV trace in Fig. 3B).

Signal and sensory functions of a complex electric field

Some of the complexity observed in the electric fields of *Brachyhypopomus* spp. appears to serve particular functions, whether by adaptation or artifact. In particular, the electric fields around the head and tail of the fish are distinctly different and we suggest that the fields around the head and tail serve different sensory and signal functions.

The spatial and temporal simplicity of the electric field around the head, as well as its low amplitude, should facilitate active electrolocation as well as the sensory aspects of communication and tracking of conspecifics. Electric field lines around the head and tip of the tail are radial and synchronous in comparison to those along the trunk and anterior tail (Fig. 8). Temporal stability of electric field lines will thus yield the sharpest and most synchronous electric image on the skin of the head. In contrast to amplitude-coding tuberous electroreceptors which occur all over the body surface, the time-coding tuberous electroreceptors (pulse markers) are found only on the anterior third of the body of *Brachyhypopomus* (Yager and Hopkins 1993). Thus, the time-coding receptors neither experience nor encode the rising transient of the second or third phases of the more complex local field on the posterior two-thirds of the body and tail.

Close to the body, electric fields attenuate gradually with distance, but beyond a body length, attenuation rates increase to the inverse square of distance (Fig. 9). Thresholds of the tuberous electroreceptors are no more than 3–6 dB below the autogenous EOD (Shumway and Zelick 1988, Yager and Hopkins 1993; Stoddard 1998). Therefore, tuberous electroreceptors should be unable to detect conspecifics beyond half a body length from the receiver (~5–15 cm) *unless* the autogenous and conspecific EODs coincide temporally (Hopkins and Westby 1986). In coincidence-based EOD discrimination and tracking, simplicity and low amplitude of the EOD near the receiver's head could be important. First, a simple autogenous waveform (i.e., monophase) produces a simpler pattern of distortion when it overlaps with that of the remote signaler. Second, the distortion produced by a remote signaler's EOD is inversely related to the amplitude of the receiver's EOD so coincidence analysis should be facilitated by the low amplitude of the EOD around the head. Thus, the observed restriction of multiphasic, high-amplitude waveforms to the posterior region may serve to protect useful sensory functions of the EOD near the head.

EOD amplitudes at the tail are an order of magnitude greater than at the head (Fig. 11). Further, EOD amplitude of male and female *B. pinnicaudatus* are nearly identical at the head, but are approximately twice as strong near the tail of the male than tail of the female (e.g., Fig. 11). Differences between head and tail amplitudes stem in part from body geometry; the anterior portions of the electric organ reside within the conductive muscle tissue of the trunk which causes significant shunting and spreading of currents within the body. In contrast, caudal portions of the electric organ are the dominant tissues of the caudal filament and are thus subject to less internal current leakage. The sex difference in EOD amplitudes at the tail suggest a specific adaptation for social signaling; higher amplitudes make most sense as adaptations to enhance the active space of the signal.

Near the head, the EOD is monophasic, or nearly so, but the EOD at the tail is strongly biphasic. Direct current imbalance in the local electric field, in combination with low discharge rates (8–16 Hz for *B.* sp. *''walteri''*, 20–70 Hz for *B. pinnicaudatus* and *B. beebei*) puts a significant fraction of EOD energy within the frequency spectrum of the ampullary electroreceptors. Unlike the gymnotiform fishes with continuous wave-type EODs, pulse fish with d.c.-imbalanced local electric fields could, in principle, use their ampullary electroreceptors for active electrolocation. The ampullary system would be expected to yield fine-scale spatial information about nearby objects but tell little about motion and rapid temporal changes. Changes in discharge rate of a d.c.-imbalanced signal produces a pronounced low-frequency modulation that may enable the medial, ampullary map segment of ELL to take a fine-grained electric ''snapshot'' of the electric field around the head. Consistent with this prediction, *B. pinnicaudatus* have been observed giving sharp EOD rate accelerations while pressing their faces up against small cavities, such as holes in rubber stoppers (P. Stoddard and C. Franchina, unpublished data). The possibility of active electrolocation by the ampullary system of *Brachy hypopomus* deserves further investigation. At the tail, the 2nd phase of the EOD is stronger than the 1st phase, but beyond half a body length, the strong head-negative 2nd phase tends to balance the head-positive phase produced by the entire electric organ (Figs. 9, 10). Thus, the fish may retain the d.c. imbalance around the ampullary receptors at the head while concealing the low-frequency energy from more distant hostile eavesdroppers such as catfish and electric eels (Stoddard 1994).

Because the region of electric activity moves rostro-caudally, and because of presumed current blocking by the swim bladder, the electric field lines rotate over the posterior 80% of the body surface. Because the trunk and tail EOD vectors change direction over the course of a single EOD, the electric images of objects near the trunk and much of the tail will be spread over a wider area of skin than images of objects near the tail. The result will be a blurring the phase-averaged electric images in the trunk and tail regions. Thus, degradation in phase-averaged electric image resolution is an apparent cost of rostro-caudal propagation (i.e., poor pathlength compensation). Rasnow (1996) showed how a rotating electric field produces a variety of images and suggested several positive features of electric field rotation – that the fish might extract object shape by comparing images at different phases. Rotating field lines may also provide clues to object depth and distance. Dorso-ventral currents produced by field rotation in the EOD of *B. beebei* may facilitate localization of objects above the head and back.

Over the anterior half of the fish, the strongest electric field vectors for each location shown in Fig. 7 correspond to the direction of best sensitivity of the tuberous electroreceptors of *B. diazi* (Yager and Hopkins 1993; McKibben et al. 1993). Over the posterior half of the fish, however, the strongest electric field vectors are outwards, whereas the tuberous receptors are most sensitive to fields aligned along the body axis of the fish. On the other hand, Fig. 8 shows that a significant fraction of the energy in the EOD along the back half of the animal is in fact aligned with the body axis. Where the electric field vectors form loops, a rostro-caudal receptor tuning axis may be a good compromise for detection of the autogenous electric field.

Methodological considerations

Only a few researchers have taken pains to record EODs of *Brachyhypopomus* with electrodes placed beyond the range of local electric field differences, either in natural bodies of water (e.g. Hopkins et al. 1990) or in large tanks with calibrated fish position error curves (e.g. Franchina and Stoddard 1999). Instead, most researchers have digitized EODs of fish placed in small aquaria or in plastic tubes with electrodes at either end. For fish with electric fields as heterogeneous as those of *Brachyhypopomus,* recording in small aquaria or plastic tubes leads to significant distortion of EOD waveform and difficulty in replication. One can extrapolate from the values shown in Figs. 9 and 11 to see that when recording electrodes lie within the heterogeneous local fields near the body, large local potentials of the tail dominate the smaller potentials of the head. Not only is a local head-tail waveform unrepresentative of that measured at a distance, but under these conditions variation in electrode-fish distance as small as a few millimeters cause enormous differences in measured EOD amplitude. Recording in a small vessel compresses the electric field, artificially amplifying both EOD magnitude and electrode placement errors. Obtaining quick, calibrated measurements of unstressed fish is difficult under field conditions, particularly so at night, but EOD waveforms and amplitudes can differ significantly between day and night and between stressed and unstressed fish (Franchina and Stoddard 1999; compare also Figs. 11 and 13 in this paper). Recording temperature is also a serious

consideration. Non-linear temperature effects make it clear that Q_{10} adjustments are not necessarily sufficient to correct for differences in recording conditions. Caputi et al. (1998) emphasize potential effects of sexual maturation on the sensitivity of the EOD waveform to temperature. Future work on EODs of *Brachyhypopomus*, and probably other electric fish as well, should take into consideration the following controllable factors that affect EOD waveform and amplitude: temperature, conductivity, tank size, electrode placement, time of day, and stress of handling and captivity.

Acknowledgements Brian Breslin measured the effects of temperature on the EOD under the supervision of PKS. We thank him for contributing his data to this paper. Mapping of *B. beebei* and *B.* sp. *"walteri"* was carried out in the laboratory of Jim Bower, who was also a gracious host to PKS. Measurements of sex differences in the EOD were obtained with the late-night assistance of Mark Kilburn and Krista Patterson. Mark Kilburn assisted in mapping the EODs of *B. pinnicaudatus*. Melita Morton and Duanne Jones assisted PKS in raising the fish to maturity. We thank two anonymous reviewers for their help in reviewing the manuscript and we remain indebted to the late Walter Heiligenberg, whose playful sense of humor as editor of JCP A initiated our collaboration. Financial support came from NSF grant IBN-9319968 to JM Bower and from FIU Foundation and NIH/NIGMS-GM08205 grants to PKS. Experiments complied with the "Principles of Animal Care" publication No. 86–23, revised 1985, of the National Institute of Health and also with current US law.

References

Albe-Fessard D, Martins-Ferreira H (1953) Rôle de la commande nerveurse dans la synchronisation du functionnement des éléments de l'organe électrique du gymnote, *Electrophorus electricus* L. J Physiol (Paris) 45: 533–546

Assad C, Rasnow B, Stoddard PK, Bower JM (1998) The electric organ discharges of the gymnotiform fishes: II. *Eigenmannia* sp. J Comp Physiol A 183(4): 419–432

Bastian J (1976a) Frequency response characteristics of electroreceptors in weakly electric fish (Gymnotoidei) with a pulse discharge. J Comp Physiol 112: 165–180

Bastian J (1976b) The range of electrolocation: a comparison of electroreceptor responses and the responses of cerebellar neurons in a gymnotid fish. J Comp Physiol 108: 193–210

Bennett MLV (1961) Modes of operation of electric organs. Ann NY Acad Sci 94: 458–509

Bennett MLV (1971) Electric organs. In: WS Hoar, DJ Randal (eds) Fish physiology, vol 5. Academic Press, New York, pp 347–491

Caputi AA, Macadar O, Trujillo-Cenóz O (1989) Waveform generation of the electric organ discharge in *Gymnotus carapo*. J Comp Physiol A 165: 361–370

Caputi AA, Silva AC, Macadar O (1998) The electric organ discharge of *Brachyhypopomus pinnicaudatus*: the effects of environmental variables on the waveform generation. Brain Behav Evol 52: 148–158

Comfort N (1990) Functional analysis of sexual dimorphism in a pulse-type electric fish, *Hypopomus*. Masters thesis, Cornell University, Ithaca NY

Crampton WGR (1996) The electric fish of the Upper Amazon: ecology and signal diversity. Doctoral Dissertation, Oxford University

Crampton WGR (1998) Effects of anoxia on the distribution, respiratory strategies, and electrical signal diversity of gymnotiform fishes. J Fish Biol 53: 502–520

Ferrari MB, McAnelly ML, Zakon HH (1995) Individual variation in and androgen-modulation of the sodium current in electric organ. J Neurosci 15: 4023–4032

Franchina CR, Stoddard PK (1998) Plasticity of the electric organ discharge waveform of the electric fish *Brachyhypopomus pinnicaudatus*. I. Quantification of day-night changes. J Comp Physiol A 183: 759–768

Franchina CR, Stoddard PK, Volmar CH, Salazar V (1998) Social stimulation elicits both sudden and gradual increases in duration and amplitude of the electric organ discharge of male gymnotiform electric fish (abstract). Proceedings of the 5th International Congress of Neuroethology, San Diego

Hagedorn M (1986) The ecology, courtship, and mating of gymnotiform electric fish. In: Bullock TH, Heiligenberg W (eds) Electroreception. Wiley, New York, pp 497–525

Hagedorn M (1988) Ecology and behavior of a pulse type electric fish, *Hypopomus occidentalis* (Gymnotiformes, Hypopomidae), in a freshwater stream in Panama. Copeia: 324–335

Hagedorn M (1995) The electric fish *Hypopomus occidentalis* can rapidly modulate the amplitude and duration of its electric organ discharge. Anim Behav 49: 1409–1413

Hagedorn M, Carr CE (1985) Single electrocytes produce a sexually dimorphic signal in South American electric fish, *Hypopomus occidentalis*, (Gymnotiformes, Hypopomidae). J Comp Physiol 156: 522–523

Hagedorn M, Heiligenberg W (1985) Court and spark: electric signals in the courtship and mating of gymnotid fish. Anim Behav 33: 254–265

Hagedorn M, Keller C (1996) Species diversity of gymnotiform fishes in Manu Bioreserve, Pakitza, Peru. In: Wilson DE, Sandoval A (eds) Manu, the Biodiversity of Southeastern Peru. Smithsonian Institution Press, Washington DC, pp 483–502

Hagedorn M, Zelick R (1989) Relative dominance among males is expressed in the electric organ discharge characteristics of a weakly electric fish. Anim Behav 38:520–525

Heiligenberg W, Altes RA (1978) Phase sensitivity in electroreception. Science 199: 1001–1004

Hopkins CD (1991) *Hypopomus pinnicaudatus* (Hypopomidae): a new species of gymnotiform fish from South America. Copeia: 151–161

Hopkins CD, Heiligenberg WF (1978) Evolutionary designs for electric signals and electroreceptors in gymnotoid fishes of Surinam. Behav Ecol Sociobiol 3: 113–134

Hopkins CD, Westby GWM (1986) Time-domain processing of electric organ discharge waveforms by pulse-type electric fish. Brain Behav Evol 29: 77–104

Hopkins CD, Comfort NC, Bastian J, Bass AH (1990) Functional analysis of sexual dimorphism in an electric fish, *Hypopomus pinnicaudatus*, Order Gymnotiformes. Brain Behav Evol 35: 350–367

Kawasaki M, Heiligenberg W (1989) Distinct mechanisms of modulation in a neuronal oscillator generate different social signals in the weakly electric fish *Hypopomus*. J Comp Physiol A 165: 731–741

Kawasaki M, Heiligenberg W (1990) Different classes of glutamate receptors and GABA mediate distinct modulations of a neuronal oscillator, the medullary pacemaker of a gymnotiform electric fish. J Comp Physiol A 10: 3896–3904

Kennedy G, Heiligenberg W (1994) Ultrastructural evidence of GABA-ergic inhibition and glutamatergic excitation in the pacemaker nucleus of the gymnotiform electric fish, *Hypopomus*. J Comp Physiol A 174: 267–280

Lorenzo D, Sierra F, Silva A, Macadar O (1990) Spinal mechanisms of electric organ discharge synchronization in *Gymnotus carapo*. J Comp Physiol A 167: 447–452

Mago-Leccia F (1994) Electric fishes of the continental waters of America. Biblioteca de la Academia de Ciencias Fisicales Matematicas y Naturales, vol XXIX. Caracas, Venezuela

McKibben JR, Hopkins CD, Yager DD (1993) Directional sensitivity of tuberous electroreceptors: polarity preferences and frequency tuning. J Comp Physiol A 173: 415–424

Rasnow B (1994) The electric field of a weakly electric fish. Ph.D. Dissertation, California Institute of Technology, Pasadena

Rasnow B (1996) The effects of simple objects on the electric field of *Apteronotus*. J Comp Physiol A 178: 397–410

Rasnow B, Assad C, Bower JM (1993) Phase and amplitude maps of the electric organ discharge of the weakly electric fish, *Apteronotus leptorhynchus*. J Comp Physiol A 172: 481–491

Rasnow B, Bower JM (1996) The electric organ discharges of the gymnotiform fishes: I. *Apteronotus leptorhynchus*. J Comp Physiol A 178: 383–396

Shumway CA, Zelick RD (1988) Sex recognition and neuronal coding of electric organ discharge waveform in the pulse-type weakly electric fish, *Hypopomus occidentalis*. J Comp Physiol A 163: 465–478

Spiro JE (1997) Differential activation of glutamate receptor subtypes on a single class of cells enables a neural oscillator to produce distinct behaviors. J Neurophysiol 78: 835–847

Stoddard PK (1994) Low-frequency electric field production and concealment in gymnotiform fish with pulsed electric organ discharges. Soc Neurosci Abstr 24: 370

Stoddard PK (1998) Detection of multiple stimulus features forces a trade-off in the pyramidal cell network of a gymnotiform electric fish's electrosensory lateral line lobe. J Comp Physiol A 182: 103–113

Stoddard PK, Rasnow B, Assad C (1995) Electric organ discharges of the gymnotiform fish *Brachyhypopomus* spp. Nervous systems and behavior. Proceedings of the 4th International Congress of Neuroethology, pp 417

Stoddard PK, Kilburn MD, Patterson KH (1996) Complex electric signal structure in reproducing gymnotiform electric fish. Soc Neurosci Abstr 22: 450

Sullivan JP (1997) A phylogenetic study of the neotropical hypopomid electric fishes (Gymnotiformes: Rhamphichthyoidea). Doctoral Dissertation, Duke University

Ticku MK (1983) Benzodiazepine-GABA receptor-ionophore complex. Current concepts. Neuropharmacology 22: 1459–70

Westby GWM (1988) The ecology, discharge diversity and predatory behaviour of gymnotiforme electric fish in the coastal streams of French Guiana. Behav Ecol Sociobiol 22: 341–354

Yager DD, Hopkins CD (1993) Directional characteristics of tuberous electroreceptors in the weakly electric fish, *Hypopomus* (Gymnotiformes). J Comp Physiol A 143: 401–414